Pro gradu – Master thesis
Physics – Atmosphere-Biosphere Studies

The effect of aerosols on long wave radiation and global warming

You Zhou

August 8th, 2015

Supervisor: Hannu Savijärvi

Evaluators: prof. Markku Kulmala and emeritus prof. Hannu Savijärvi

UNIVERSITY OF HELSINKI
DEPARTMENT OF PHYSICS

PL 64 (Gustaf Hällströmin katu 2)
00014 University of Helsinki

Foreword

I studied for my master's degree about 5 years between 2010-2015. The journey was tough at times, but I am happy with the end result. After receiving my master's degree I plan to continue my life in Helsinki as an entrepreneur doing trading between Finland and China, focusing on environmental and aerosol technologies. I would like to express my thanks to all of the people who supported me and provided advice during these five years. This wouldn't have been possible without your support.

Firstly, I would like to thank my supervisor, Professor Hannu Savijärvi, who gave me a chance to write this master's thesis and the related scientific publication with him. My background studies in both meteorology and aerosol physics were limited before this work, but my supervisor was really patient and understanding when advising me. Further, I would like to say thank you to my degree supervisor Professor Markku Kulmala, Professor Timo Vesala, Dr. Antti Lauri and everyone else who gave me advice to finalize this thesis.

Secondly, I would like to thank my best friend Daniel Hirschberg, who now lives and works in Sweden as a medical doctor. Despite living in different country, he continued to give me his best support throughout the five years. We call each other often and we are always willing to listen and support each other when one of us is undergoing difficult times. I had a severe illness for 2-3 years during the last five years. He helped me a lot during my long recovery, both through his friendship and his medical knowledge.

Finally, I would like to say thank you to all my family members. I have been away from home for most of this time and both I and my family members have lost a lot of precious time and many important moments together. I would also like to thank my Finnish boyfriend and his family who have accompanied me and given me invaluable mental support during the 2-3 years I was sick, never giving up believing in me and supporting me even when things were at their worst.

I believe happiness will come if you never give up. Life is fair for everyone. One shouldn't worry about loss, because there will gain after that. When God closes one door, at the same time he will open the next door. If you are reading my thesis, I hope you have a good time in University of Helsinki and Finland. Best wishes.

Helsinki

10.6.2015

You Zhou

ABSTRACT

Long wave (LW) radiation in the Earth's atmosphere is defined as the radiation at wavelengths longer than 4 μm (infrared). The short wave (SW) radiation wavelengths are less than 4 μm (visible light, ultraviolet). SW radiation is usually from solar origin. The absorbed solar SW radiation is closely balanced by the outgoing LW radiation in the atmosphere. This radiation balance keeps the global average temperature stable.

The main cause of the current global warming trend is human expansion of the 'greenhouse effect'. Atmospheric greenhouse gases absorb the thermal LW radiation from a planetary surface. The absorbed radiation is re-emitted to all directions. Some of the energy is transferred back to the surface and the lower atmosphere since part of the re-radiation is directed towards the surface, resulting in increased surface temperature.

The local radiation balance is also affected by clouds and aerosols in the atmosphere since they too can absorb and scatter radiation. The effects of clouds and greenhouse gases on the global radiative balance and surface temperature are well known. The aerosols, however, are one of the greatest sources of uncertainty in the interpretation and projection of the climate change. Natural aerosols such as those due to large eruptions of volcanoes and wind-blown mineral dust are recognised as significant sources of climate forcing. In addition, there are several ways in which humans are altering atmospheric aerosols. These include industrial emissions to the lower atmosphere as well as emissions to as high as lower stratosphere by aircraft.

In this thesis the effect of aerosols on LW radiation was studied based on narrowband LW calculations in a reference mid-latitude summer atmosphere with and without aerosols. Aerosols were added to the narrowband LW scheme based on their typical schematic observed spectral and vertical behaviour over European land areas. This was found to agree also with spectral aerosol data from the Lan Zhou University Semi-Arid Climate Observatory and Laboratory measurement stations in north-western China.

A volcanic stratospheric aerosol load was found to induce local LW warming with a stronger column “greenhouse effect” than a doubled CO_2 concentration. A heavy near-surface aerosol load was found to increase the downwelling LW radiation to the surface and to reduce the outgoing LW radiation, acting very much like a thin low cloud in increasing the LW greenhouse effect of the atmosphere. The short wave reflection of white aerosol has, however, stronger impact in general, but the aerosol LW greenhouse effect is non-negligible under heavy aerosol loads.

KEYWORDS

Aerosols, long wave radiation, radiative forcing, long wave heating rate, long wave radiation scheme, Lan Zhou city, climate change

Table of Contents

Nomenclature

Alphabets

B_k	blackbody spectral radiance
c	speed of light in vacuum
C_p	specific heat capacity at constant pressure p
g	standard acceleration
h	hemisphere
H	scale height
I	energy flux intensity
j	emission coefficient
k	wave number
$\boldsymbol{K}$	short wave flux
$\boldsymbol{L}$	long wave flux
p	pressure
q	water vapor mixing ratio
$\boldsymbol{Q}$	net radiative energy
$\boldsymbol{s}$	position
t	flux transmittance
t_a	aerosol flux transmittance
t_{gas}	greenhouse gas flux transmittance
T	temperature
T_0	surface temperature
V	horizontal meteorological visibility
z	altitude

Special symbols

α	wavelength exponent
α_k	absorption coefficient at wave number k
β	Ångström turbidity parameter
β_{ae}	aerosol volume extinction coefficient
ε	emissivity
σ_s	scattering cross section
σ_a	absorption cross section

λ	wavelength
μ	cosine of the zenith angle
μ_1	inverse of the diffusivity factor
ρ	density
σ	Stefan-Boltzmann constant
τ	optical depth
τ_a	aerosol optical depth
Ω	solid angle

Abbreviations

AOD	vertical aerosol optical depth
CCN	cloud condensation nuclei
CRF	cloud radiative forcing
DLR	downwelling long wave radiation at the surface
ICRCCM	International Comparison of Radiation Codes in Climate Models
LHR	long wave heating rate
LBL	line-by-line
LW	long wave
LWP	liquid water vertical path
MLS	mid-latitude summer
NBM	narrow-band model
NO_x	nitrogen oxides
OLR	outgoing long wave radiation
PM	fine particulate matter
SACOL	Semi-Arid Climate Observatory and Laboratory
SW	short wave

1 Introduction

The Earth is in a near radiation balance, the outgoing long wave (thermal) radiation (OLR) closely balancing the absorbed solar radiation. Transfer of energy in the form of electromagnetic radiation, commonly known as radiative transfer plays a significant role in the dynamics of the Earth's atmosphere and the climate. The radiation changes through scattering, absorption and emission in the atmosphere. This transfer of energy also affects the air temperature. Greenhouse gases, clouds and dust in the atmosphere have influence on the radiative transfer and through it the climate, since they absorb, scatter and emit radiation. This process, known as radiative forcing, is described in Fig. 1.

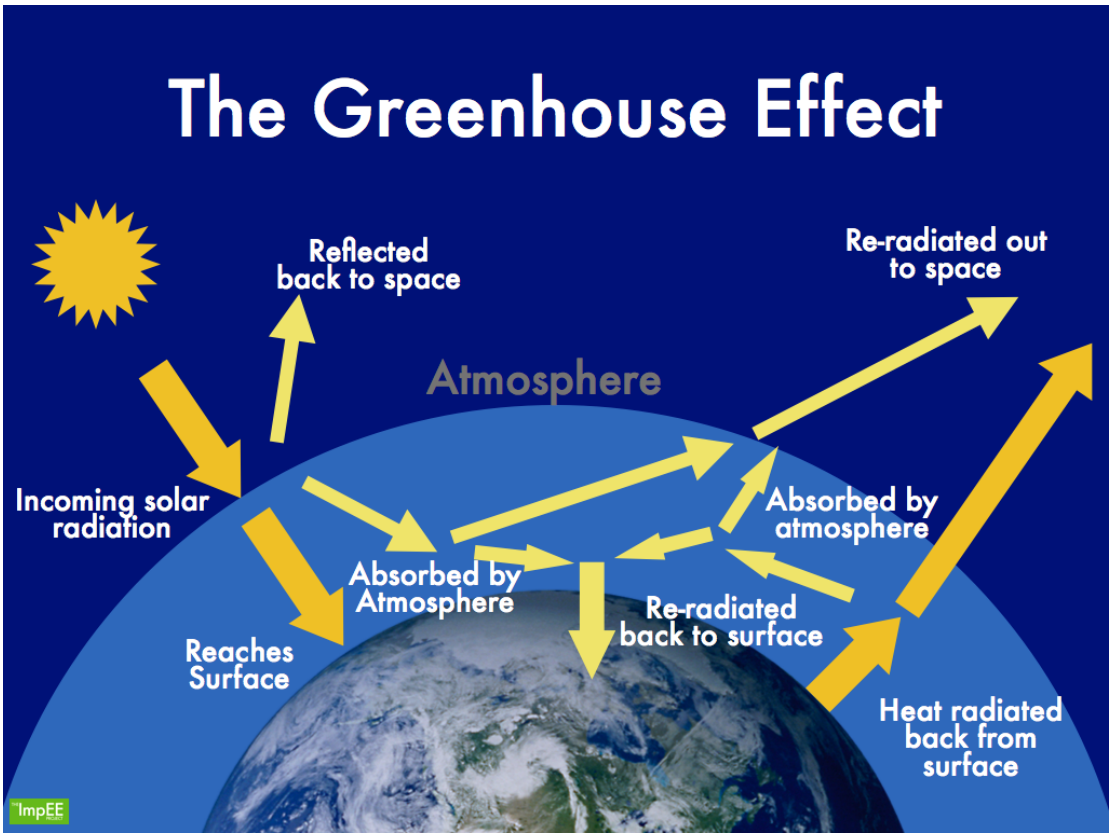

Figure 1: The radiative forcing process (Greenhouse effect, 2011). Clouds, greenhouse gases and airborne aerosols all influence the climate by changing the amounts of absorbed, reflected or re-radiated SW and LW radiation. Radiative forcing of greenhouse gases, 'greenhouse effect', is the most important cause of the current global warming trend. The effects of clouds and aerosols are generally more local.

The main cause of the current global warming trend is human expansion of the 'greenhouse effect'. Thermal radiation from a planetary surface is absorbed by atmospheric 'greenhouse gases' (CO_2, methane, water vapour, etc.), and is re-radiated (emitted) into all directions. Since part of this re-radiation is back towards the surface and the lower atmosphere, it results in an elevation of the average surface temperature above what it would be in the absence of the greenhouse gases. Recent studies show that the levels of several important greenhouse gases have increased by about 25 percent since large-scale industrialization began around 150 years ago. As a result, Earth's mean surface temperature has increased by about 0.8 °C, with about two-thirds of the increase occurring since 1980. During 21st century, the mean surface temperature is expected to rise 1.1 °C – 6.4 °C depending on the applied emission scenario (Hartmann, 1994).

The effect of clouds on OLR and on the cloud radiative forcing (CRF), can be estimated from satellite data by taking the difference between the clear sky scenes and all scenes (table 1). These observations indicate that clouds increase the planetary shortwave (SW) albedo by 15% to 30%, thereby reducing the absorbed solar radiation by about 48 W/m^2. This cooling effect is opposed by the warming effect of clouds on the longwave (LW) radiation (the "cloud LW greenhouse effect"), which reduces the clear sky OLR by about 31 W/m^2 on the average (Hartmann, 1994).

Table 1: Cloud radiative forcing as estimated from satellite measurements (W m^{-2}) (Hartmann, 1994).

	Average	Cloud free	Cloud forcing
OLR	234	266	31
Absorbed solar radiation	239	288	-48
Net radiation	5	22	-17
Albedo	30%	15%	15%

This study concentrates on the analogous long wave radiative effect ("LW forcing") of airborne aerosols (other than clouds), which is less well-known than that of the

clouds or the greenhouse gases. During the 1970s, the influence of the aerosol layer height and the changes of surface albedo on the atmospheric radiation balance were investigated by Reck (Reck, 1974, 1975). The results of those pioneering studies showed that like the clouds, aerosols produce two opposing effects in the atmosphere: They cause heating of the Earth's surface by enhancing the downwelling LW radiation, but they also increase the planetary SW albedo, which causes a cooling effect. The combined effect depends on many factors including the aerosol particle type, concentration and height. It also varies on time due to the diurnal and seasonal changes in the incoming solar radiation. The cooling effect due to a reduction of the incoming solar radiation often dominates at daytime while the weaker warming effect due to the aerosol LW emission is present throughout the day and may be observed at night time.

In the 1980s, new methods were developed for investigating the aerosol characteristics and their effects on the albedo and climate. These include e.g. the multi-wavelength satellite extinction measurements (Lenoble, 1986), and balloon or aircraft measurements. At the same time the focus also turned towards the effects of volcanic aerosol loads in the stratosphere as well as to the effects of aerosols on the local climate in specific locations. The latter was investigated e.g. in the city of St. Louis, USA, by Method and Carlson (1982). These studies showed that the effects of aerosols are similar to those of a thin cloud at the same height. However, the impact is small in magnitude and difficult to measure unless the aerosol concentration is extremely high. The 1990s saw significant increase of research on aerosols and their effect on climate. First computer models of the effects of aerosols on the radiation balance were developed. One such model is presented by Claquin et al. (1997).

In the 21st century, the work of studying and understanding the effects of both natural and man-made aerosols on the radiation balance both globally (Dammann et al., 2000) and locally (Shaocai et al., 2001; Han et al., 2012) has continued. The effects of specific types of aerosols or effects of aerosols in specific locations have also been studied (Verma et al., 2006; Wendisch et al., 2008). More recently, the radiative effects of aerosols have been studied in both urban and remote areas of western India in 2011 (Ramachandran et al., 2011), Europe (Péré et al., 2012), USA (Mickley et al., 2012) and China (Zhang et al., 2012). The results show significant variability of the

radiative effects due to the meteorological conditions as well as the aerosol loads themselves. Therefore the aerosol processes and meteorological processes appear to be coupled and they interact with each other. This is best studied by using atmospheric and radiative models equipped with aerosol schemes, and simultaneously using surface, aircraft and satellite measurements. In this way, for instance, the major Saharan dust storms have been shown to imply considerable differences into the surface LW fluxes and OLR (Haywood et al. 2005; Slingo et al. 2006; Hansell et al. 2010). However, such coupled studies, although the most complete, are dominated by the strong daytime SW effects of the aerosol, and so may not be optimal in isolating and characterizing the LW effects and mechanisms.

Therefore, in this study the OLR differences, the LW surface budget differences and the internal LW heating/cooling rates are studied by comprehensive narrowband LW model calculations, using various controlled aerosol loads in typical mid-latitude conditions. In particular, the observed aerosol loads of north-western China are used as an extreme example, because the wind-blown mineral dust storms from the surrounding deserts and the heavy industrial pollution in the city of Lan Zhou provide quite large natural and anthropologic aerosol loads for this region. In general, pollution in South-East Asia is increasing rapidly, the visibility in the larger cities being reduced due to the heavy aerosol loads, satellite observations even revealing large impacted areas ("the Asian brown cloud"). Hence the aerosol LW forcing may become stronger there in the near future, and eventually at least regionally, perhaps even globally, important for the climate.

Here, detailed quantitative LW calculations were made in a typical mean mid-latitude summer air column (Ellingson et al., 1991) using a validated, rather accurate narrow-band spectral LW scheme (Savijärvi, 2006), and introducing variable aerosol, cloud, and greenhouse gas loads into the scheme. The results for the different cases were compared. The aerosol effects with different aerosol amounts and profiles were analysed for the OLR, for the downwelling LW radiation at the surface (DLR), and for the resulting internal LW heating rates in the atmosphere (LHR).

1.1 Theoretical background

Atmospheric radiative transfer is a discipline that studies the radiation energy transfer and conversion processes in the Earth's atmosphere. Atmospheric radiation transfer theory is based on the theory of molecular spectroscopy and electromagnetic wave propagation at different wavelengths λ. The radiative transfer process is a basic factor affecting the climate and atmospheric circulation.

The research in atmospheric radiative transfer includes three main topics: First topic includes the basic physical processes and rules of radiative transfer in the Earth's atmosphere, including SW radiation, LW radiation, and their absorption, scattering and emission in the atmosphere by water vapor, O_3, CO_2 and other gases. Clouds, aerosols and the surface of the Earth also have influence on the radiative transfer. The second topic is the radiative transfer equation itself. It describes the interaction between the radiation and the medium when there is absorption, scattering and emission of radiation. The radiative transfer equation is not difficult to derive, but using it in the actual Earth's atmospheric conditions requires some highly simplified assumptions in order to obtain analytical solutions. Seeking more accurate physical and numerical approximations of the radiative transfer equation in the real atmosphere deconstruction is therefore an important research subject in the atmospheric radiative transfer. The third topic is the research related to the relationships between the atmospheric radiation, weather and climate. This includes studies of the thermodynamic effects based on the observed radiation budget of the Earth's atmosphere (such as Table 1), studying the effects of radiation on the formation of weather and climate, and the climate change research.

The following brief review of radiative transfer follows Liou's (1992) textbook conventions. (Liou, KN, 1992: Radiation and cloud processes in the atmosphere. Oxford University Press, Oxford, 487 pp.)

1.1.1 Radiative transfer equation

The equation of radiative transfer can be written as

$$\frac{1}{c}\frac{\partial}{\partial t} I_k + \hat{\Omega}\cdot\nabla I_k + (\sigma_{k,s} + \sigma_{k,a}) I_k = j_k + \frac{1}{4\pi c}\sigma_{k,s}\int_{\Omega} I_k d\Omega, \qquad (1)$$

where I_k is the energy flux in the solid angle $d\Omega$ in the wave number interval k to $k+dk$, j_k is the emission coefficient, $\sigma_{k,s}$ is the scattering cross section, $\sigma_{k,a}$ is the absorption cross section, and $k = 1/\lambda$. The first two terms on the left side of the equation, respectively, are time rate of change of the radiation flux and the rate of energy transfer along the direction of $\boldsymbol{\Omega}$. The third term on the left is the absorption and outscattering term, which gives the fraction of the radiation that is absorbed or scattered away. The two source terms on the right are the emission and inscattering terms respectively. They give the amounts of radiation emitted and "gained" by scattering. Solutions to Eq. 1 are often very difficult to obtain. This is mainly due to the various forms for the emission, absorption and scattering coefficients.

If scattering is ignored ($\sigma_{k,s} = 0$), which is a good approximation in the LW range, then a general solution to Eq. 1 in terms of the emission and absorption coefficients can be written as:

$$I_k(s) = I_k(s_0)e^{-\tau_k(s_0,s)} + \int_{s_0}^{s} j_k(s')e^{-\tau_k(s',s)}ds', \qquad (2)$$

where $\tau_k(s_1,s_2)$ is the optical depth of the medium between positions s_1 and s_2. The energy flux I_k at s_0 is determined from a boundary condition. $\tau_k(s_1,s_2)$ is defined as

$$\tau_k(s_1,s_2) \equiv \int_{s_1}^{s_2} \alpha_k(s)ds, \qquad (3)$$

where $\alpha_k(s)$ is the absorption coefficient of the medium for wave number k at position s. Eq. 2 can be simplified by assuming local thermodynamic equilibrium. In this approximation, which is valid below about 80 km heights in the Earth's atmosphere, the particles in an air parcel are assumed to be in thermodynamic equilibrium with each other and therefore share the same temperature. For such a medium $\alpha_k = \varepsilon_k$, and $\boldsymbol{j_k}$ follows the Planck's law of blackbody radiation

$$j_k = \varepsilon_k B_k(T), \qquad (4)$$

where ε_k is the source emissivity at wave number k and $B_k(T)$ is the blackbody spectral radiance, also known as the Planck function, at temperature T. The solution to Eq. 1 in local thermodynamic equilibrium and assuming no scattering can therefore be written by combining Eq. 2 and Eq. 4:

$$I_k(s) = I_k(s_0)e^{-\tau_k(s_0,s)} + \int_{s_0}^{s} B_k(T(s'))\alpha_k(s')e^{-\tau_k(s',s)}ds' \quad (5)$$

Eq. 5 can be further simplified by writing it in terms of a flux transmittance t_k:

$$t_k(s,s') = e^{-\tau_k(s,s')} \quad (6)$$

$$I_k(s) = I_k(s_0)t_k(s_0,s) + \int_{s_0}^{s} B_k(T(s'))\frac{\partial t_k(s,s')}{\partial s'}ds' . \quad (7)$$

Total flux along the direction of the solid angle $\boldsymbol{\Omega}$ at wave number k can be obtained from Eq. 7 by integrating $I_k(s)$ over $\boldsymbol{\Omega}$. In general this integration cannot be done in closed form, however, and another approximation must be considered. In the plane-parallel case a widely used and fairly accurate approximation in the LW range is the diffusivity approximation, first suggested by Elsasser in 1942:

$$t_k(\tau_k) = 2\int_{\pi/2}^{0} \frac{e^{-\tau_k/\mu}}{\mu}d\mu \approx e^{-\frac{\tau_k}{\mu_1}}, \quad (8)$$

where μ is the cosine of the local zenith angle and $1/\mu_1 = 1.66$ is the diffusivity factor. Using this the LW fluxes ($L_{k,up}$ and $L_{k,down}$) can be written by integrating Eq. 7 over the hemisphere up and down respectively:

$$L_{k,up}(z) = \left\{\varepsilon_k \pi B_k(T_0) + (1-\varepsilon_k)L_{k,down}(0)\right\}t_k(0,z) + \int_0^z \pi B_k(T(z'))\frac{dt_k(z,z')}{dz'}dz' \quad (9)$$

$$L_{k,down}(z) = \int_{\infty}^{z} \pi B_k(T(z'))\frac{dt_k(z,z')}{dz'}dz', \quad (10)$$

where $T(z)$ is the mean temperature of the layer of air at height z and ε_k is the ground emissivity at wave number k. In Eq. 9, a boundary condition that $L_{k,up}(0)$ consists of the thermal blackbody radiation from the ground and the reflected downwelling radiation was applied. $L_{k,down}(\infty)$ is assumed to be 0.

1.1.2 Long wave and short wave radiation

LW radiation in the Earth's atmosphere is defined as the radiation at wavelengths λ longer than 4 μm. It is usually emitted by the Earth's surface and by the atmosphere itself, and is therefore of terrestrial origin. The SW radiation wavelengths are less than 4 μm and are usually of solar origin. Fig. 2 shows the typical spectral distributions of SW and LW radiation at the top of the Earth's atmosphere.

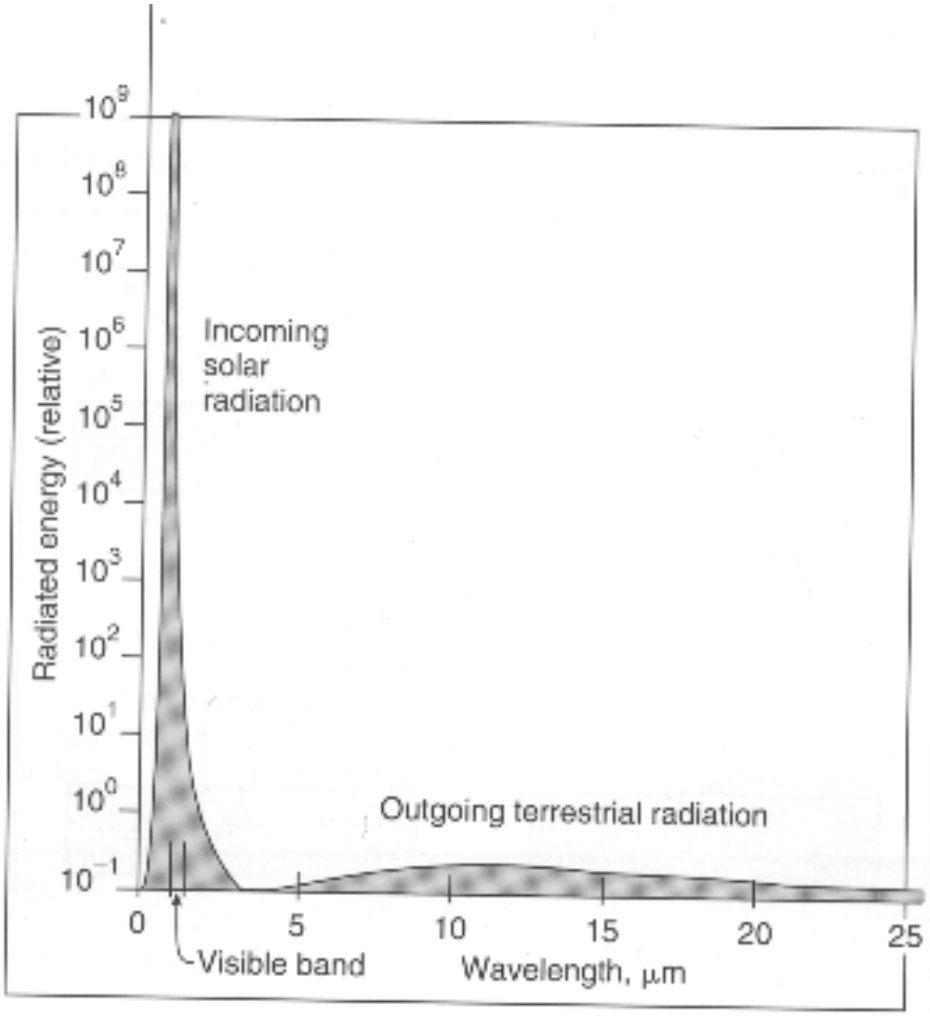

Figure 2: The wavelength ranges of the outgoing terrestrial (long wave) radiation and incoming solar (short wave) radiation. (DeLiberty, 1999)

As the SW and LW radiation propagate through the atmosphere, part of the radiation is absorbed or scattered. When SW and LW radiation is absorbed at the surface or in the atmosphere, part or most of its energy is re-emitted as LW radiation. Energy is conserved. Therefore Earth and its atmosphere are in a radiation balance, which can be expressed with the radiation budget equation

$$Q = K_{net} + L_{net} = (K_{down} - K_{up}) + (L_{down} - L_{up}), \tag{11}$$

where K is the SW flux, L is the LW flux and Q is the net radiative energy that is absorbed and then transformed into a non-radiative form. This can result in changes in air, ground and ocean temperatures, or evaporation or condensation of water. The radiative balance (Eq. 11) can be formed at any level at the surface or within the atmosphere. The radiative heating rate at altitude z can be calculated from the vertical convergence of the net flux $Q(z)$:

$$\frac{\partial T}{\partial t}(z) = \frac{1}{\rho C_p}\frac{\partial Q}{\partial z} = -\frac{g}{C_p}\frac{\partial Q}{\partial p}, \tag{12}$$

where ρ is the air density, C_p is the specific heat capacity of air at constant pressure p, g is the Earth's standard acceleration due to gravity and the last form follows from the hydrostatic relation. At the top of the Earth's atmosphere, where the air is very thin, $\partial Q/\partial z$ is zero.

SW radiation is emitted from the Sun and then transmitted through the atmosphere. The incoming SW flux therefore depends on the solar altitude as well as the transmissivity of the atmosphere above. Outgoing SW radiation consists of SW radiation that is reflected in the atmosphere or at the surface. Its flux depends on the incoming SW flux and the albedo of the atmosphere below and of the surface. The SW fluxes vary greatly depending on the time of the day, time of the year, clouds, latitude, terrain, surface albedo etc., but on the average about 30% of the total incoming SW radiation is reflected back to space (global albedo = 0.30, table 1), 25% is absorbed in the atmosphere and 45% is absorbed at the surface.

LW radiation is emitted by the surface and air into all directions. For a medium in (local) thermodynamic equilibrium, this emission follows Eq. 4 and therefore depends on temperature and emissivity of the source. The total power emitted per unit area of the source can be calculated by integrating the emission coefficient j_k over the hemisphere h above the surface element and over the whole wave number range from 0 to ∞, giving

$$\int_0^\infty dk \int_h d\Omega \varepsilon_k B_k(T)\mu = \varepsilon\sigma T^4, \tag{13}$$

where μ is the cosine of the angle to the surface element normal, ε is the broadband emissivity and σ is the Stefan-Boltzmann constant.

Ground is the main direct heating source of the troposphere. Its LW emission depends on the surface temperature and emissivity according to Eq. 13, the ground emissivity being close to 1. In general, 75% to 95% of the LW emission of the ground is absorbed in the troposphere by water vapor, CO_2, O_3 and other greenhouse gases. O_2 and N_2 on the other hand are transparent to LW radiation. The absorbed energy is re-emitted at the air temperature to all directions. Part of this emission is back towards the ground, which creates the 'greenhouse effect'. On the average about 70% of the total radiative energy is lost to space and 30% is transformed into a non-radiative form.

Temporal and spatial variability of the SW and LW fluxes is significant. At night-time, incoming SW flux K_{down} is zero, which results in a negative radiation balance (Q). At daytime, higher solar altitude near the equator than near the poles results in greater K_{down} at low latitudes. K_{down} is also greater during summer than winter at higher latitudes for the same reason. Terrain also has an effect on the radiative fluxes. Higher elevation means less atmospheric absorption for both SW and LW radiation and results in higher Q at daytime and more negative Q at nighttime. South facing slopes at northern hemisphere also receive more incoming SW radiation than north facing slopes, which results in higher Q at daytime. This situation is reversed in the southern hemisphere. Surfaces with high albedo, such as snow and glaciers, reflect more SW radiation back to the atmosphere than darker surfaces, which results in higher K_{up} and lower Q at daytime. Temporal and spatial variations in cloud cover, dust and pollutants also affect the radiation balance by reflecting both SW and LW radiation. At daytime the reflection of SW radiation dominates, which results in decreased Q from the clear sky conditions. At nighttime, absorption and re-emission of the outgoing LW radiation (L_{up}) results in less negative Q from the clear sky conditions.

1.1.3 Aerosols and greenhouse gases in the Earth's atmosphere

Fig. 3 shows the different layers of the Earth's atmosphere. The lowest layer is the troposphere, which contains about 80% of the atmospheric mass and about 99% of its

water vapour and aerosols. Most of the phenomena that affect surface weather occur in the troposphere. The depth of the troposphere varies with latitude and season. It is about 10-13 km at mid-latitudes and 7-8 km at the poles. At the equator the troposphere can be as thick as 18 km. The stratosphere is located above the troposphere and below the mesosphere. It starts from the top of the troposphere, tropopause, and extends to about 50 km above the surface. The most important absorbers and emission sources of LW radiation, greenhouse gases and aerosols, are concentrated in the troposphere and the stratosphere.

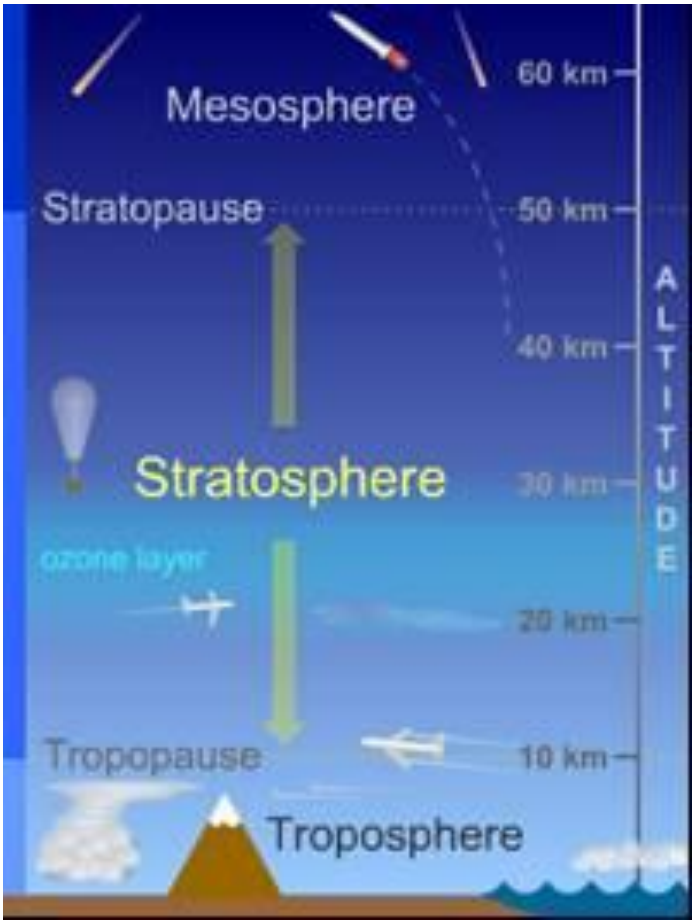

Figure 3: The layers of the Earth's atmosphere.

1.1.3.1 Greenhouse gases

Greenhouse gases are gases in the atmosphere that absorb and emit radiation in the thermal infrared range. The primary greenhouse gases in the Earth's atmosphere are water vapor, CH_4, CO_2, N_2O, NO_x and O_3. The abilities of each of these gases to

absorb and emit radiation in the LW range are different. For instance, water vapour is a strong absorber while CO_2 and O_3 are weaker absorbers. NO_x and CH_4 are both strong greenhouse gases, but they are also less abundant than for example CO_2. Greenhouse gases typically absorb and re-emit 75% - 95% of the total LW radiation emitted from the ground. Without them, the average temperature of the Earth's surface would be about 33°C colder than its present value of 14°C.

The absorption and re-emission of LW radiation due to the greenhouse gases is sharply selective since it takes place at quantized rotational and vibrational energy level changes of the multi-atom molecules, showing up in the form of numerous spectral peaks called lines. As can be seen from Fig. 4, the absorption spectra of the different greenhouse gases are very complex. The strongest LW absorption occurs in the wavelength ranges 5 μm - 8 μm and above 18 μm (water vapor), 13 μm – 17 μm (CO_2), and 9 μm – 10 μm (O_3). The atmosphere is most transparent to LW radiation in the atmospheric LW windows at wavelengths 8 μm – 12 μm and 17 μm – 18 μm. The LW spectrum from clouds (water drops; ice particles) is broadly similar to the spectrum of water vapour, but the absorption is stronger. Dense clouds are virtually opaque to LW radiation, acting as blackbodies.

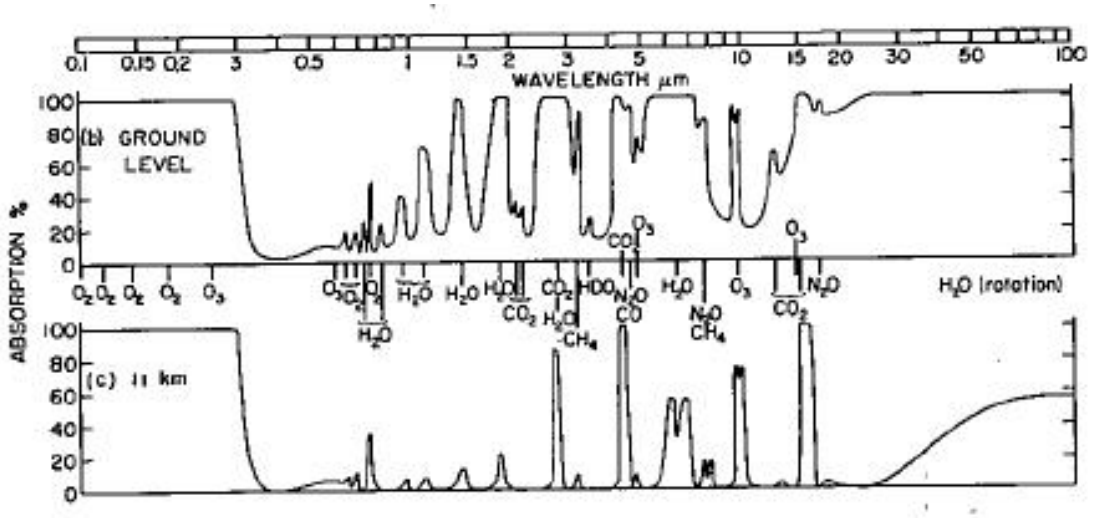

Figure 4: Gas transmissivities for the whole atmospheric column, and above 11 km, showing the LW window at 8-12 μm between the H_2O and CO_2 absorption bands. (Hartmann, 1994)

The radiative transfer in Earth's atmosphere is modelled with the radiative transfer equation (Eq. 1). In order to calculate the radiation budget for a specific spectral region, Eq. 1 must be integrated over the wave number range of interest. The main

computational problem is representing the strong spectral variation of the flux transmittance t_k for the millions of absorption/emission lines of the greenhouse gases in each layer of air. The most exact way to do this is the line-by-line (LBL) calculation, which means calculating the contribution of each spectral line of all gases in the atmospheric layer on α_k and t_k. A faster but more approximate method is the band transmission method, in which t_k in a band is characterized by the distribution of lines within the band, using a set of lab-observed coefficients that depend on temperature and other parameters. The most commonly used statistical line distributions ("random band models") are by Goody and Malkmus (Houghton, 2002). Many different radiative transfer models using both of these methods have been developed. Some of these models also take into account the scattering from molecules and particles as well as polarization, but in the LW range these effects are insignificant for our application. Models using the LBL integral method are more accurate, but also much slower than the band models. Therefore LBL models are often used as a reference to test other, more approximate models.

1.1.3.2 Aerosol particles

An aerosol is a suspension of fine solid particles or liquid droplets in a gas. The diameter of the typical particles is between 0.01 μm to 10 μm. There are three ways by which the atmospheric aerosols can influence the climate: Firstly, aerosol particles influence the climate directly through their absorption and scattering of solar radiation, by changing the SW energy budget of the Earth and atmosphere system. Secondly, aerosol particles indirectly influence the climate by forming cloud condensation nuclei (CCN) and thus changing the optical properties, distribution and life cycle of clouds. Thirdly, the aerosols also influence the thermal (LW) radiation field of the planet, changing the OLR, DLR and LHR. This least known third effect is studied in this work.

About 10% of the land area of the Earth is desert. Wind-blown mineral dust and sand particles are the major components of tropospheric natural aerosol at and near such areas. The annual average amount of mineral dust in the Earth's atmosphere is about 50-250 Mt. Industry, heating and traffic of major cities are also significant

anthropogenic sources of local aerosol load, pollution. In addition, volcanic eruptions may produce natural ash, soot and sulphur-based aerosol to the stratosphere.

Aerosols can be added to the radiative transfer models by determining the aerosol volume extinction coefficient β_{ae} (km^{-1}) and calculating the aerosol vertical optical depth (AOD; $\tau_{a,k}$) and the aerosol flux transmittance $t_{a,k}$ with Eq. 3 and Eq. 6. In the LW range scattering can be ignored, so $\alpha_k = \beta_{ae}$, and the diffusivity approximation (Eq. 8) can be used for the determination of $t_{a,k}$.

The observations of the typical schematic behavior of aerosols over inland areas show that β_{ae} (km^{-1}) often follows approximately the equation

$$\beta_{ae}\left(z,\lambda,V\right) = 0.2\,km^{-1}\left(\frac{20\,km}{V}\right)\left(\frac{0.55\,\mu m}{\lambda}\right)e^{-\left(\frac{z}{H}\right)}. \qquad (14)$$

The aerosol concentration is hence assumed to decay upward exponentially with a scale height H (~1 km). At the surface β_{ae} is 0.2 km^{-1} at the reference visible wavelength λ = 0.55 µm when the horizontal meteorological visibility V is 20 km, and it is assumed to be inversely proportional to both V and λ. These assumptions were verified here using data from many careful spectral aircraft and tower observation campaigns of aerosols made around the north-western China and in the city of Lan Zhou (Sect. 2). The observations were made at the Semi-Arid Climate Observatory and Laboratory (SACOL) stations of the University of Lan Zhou.

The near surface values of β_{ae} at λ = 9 – 10 µm (within the LW window region) are about 0.01 km^{-1} from Eq. 14 during the typical visibility of 20 km. This agrees with spectral LW observations and other continental LW aerosol models in the literature (See e.g. Table 9.2 and Fig 9.9 in Paltridge and Platt, 1976).

Alternatively in the calculations that follow in Sect. 4, one has assumed a vertically constant ("well-mixed boundary layer") concentration of aerosols (i.e. Eq. 14 without the exponential term), to a certain height (~0.5-2 km).

The combined transmissivity of aerosols and greenhouse gases for each layer and each wave number or wave number band is

$$t_k = t_{gas,k} \cdot t_{a,k} \quad (15)$$

Thus the aerosols are ineffective in opaque gaseous bands, where t_{gas} ~ 0, and have their biggest impact in the LW window, where t_{gas} ~ 1.

1.1.3.3 Differences between aerosol particles and greenhouse gases

The life assessment studies of the aerosols and greenhouse gases show that lifetimes of tropospheric aerosols range from a few days to a few weeks, depending on their composition, distribution and concentration as well as the altitude and weather conditions (Li and Fan, 2006). The particles with diameter between 0.1 μm to 10 μm tend to have the longest lifetimes. The radiative forcing effects of the short-lived urban and continental aerosols stay mostly near their emission sources, so they essentially affect only the northern hemisphere. On the other hand, the lifetime of greenhouse gas molecules is tens or hundreds of years, and they influence the whole atmosphere.

Atmospheric aerosols influence the solar radiation during the daytime, so their shortwave impact is greatest at low latitudes and during summer. In contrast, the greenhouse gases and aerosols affect the thermal radiation both in daytime and night time. They have influence also during winter and in the middle and high latitudes. The effect of the aerosol particles on SW radiation also depends significantly on the optical properties of the underlying surface reflecting the sunshine. The impact of greenhouse gases is not affected by those. Aerosols also act as CCN, and they can thereby influence the climate indirectly through the changes in the clouds (Li and Fan, 2006). The greenhouse gases do not have such an indirect effect.

1.2 Aerosol particle pollution in north-western China and the city of Lan Zhou

About 1/4 of the land area of China is desert. Wind-blown dust and sand are therefore major components of the air pollution in China. The mineral dust aerosol particles influence heavily the air quality of 12 major Chinese cities and provinces. Despite the local pollution by industry, heating and traffic within cities, the mineral dust is

probably the main problem especially in the north-western China and everywhere in the more rural areas.

The city of Lan Zhou (36º02' N, 103º48' E) has the worst air quality among all the cities in China. It is among the 30 most polluted cities in the world. The map in Fig. 5 shows the location of Lan Zhou in China. It is close to the north-western desert areas, from where the winds often bring in mineral dust aerosol. The population of about 1 million and heavy industry also produce a large man-made aerosol load locally. In addition, the city is located in the Yellow River canyon, which makes it a "smog trap" (Savijärvi and Jin, 2001). Lan Zhou is often heavily suffering from sandstorms, which means that the concentration of mineral dust is particularly high. During a sand storm, the minimum horizontal visibility *V* in Lan Zhou can be as low as 300 m (Fig. 6).

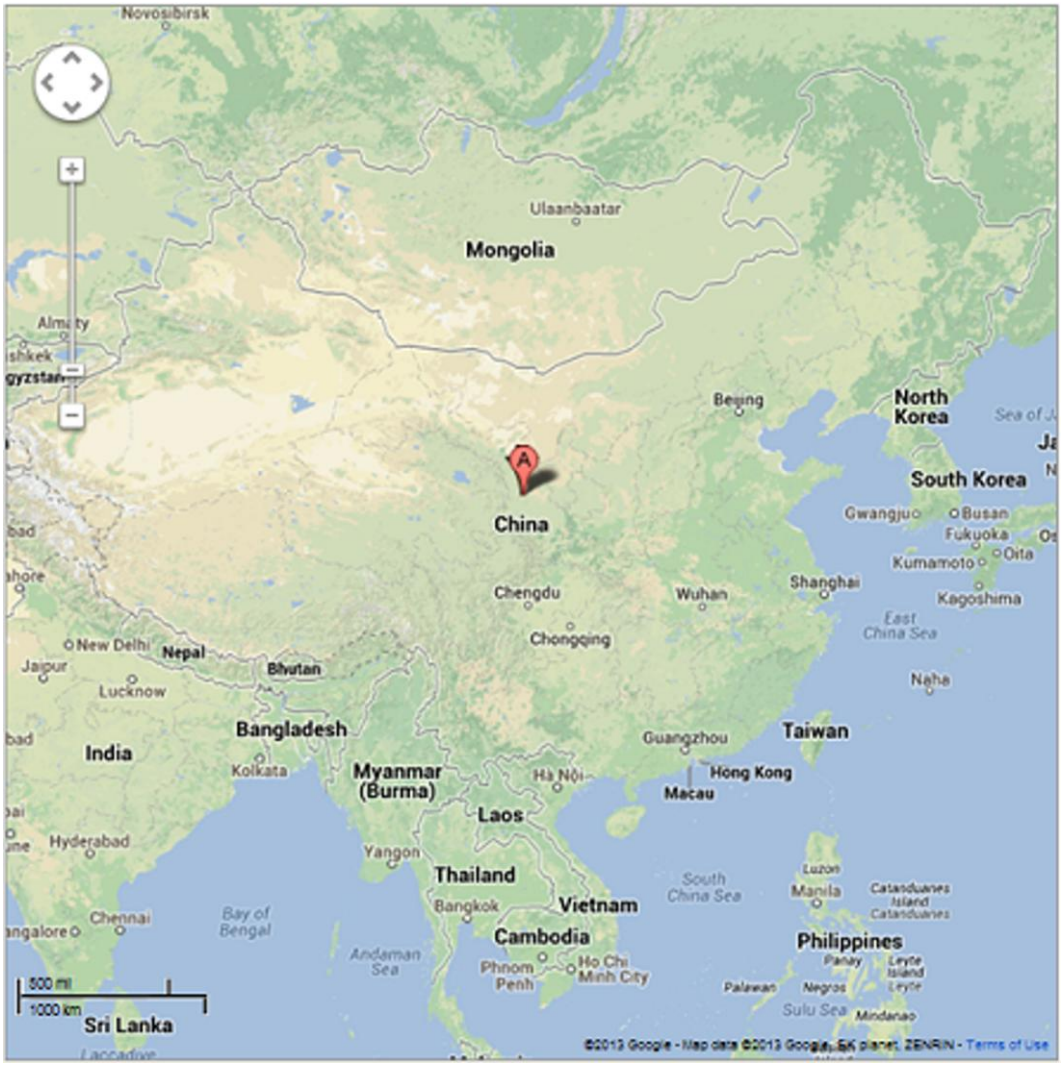

Figure 5: The location of Lan Zhou city in China.

Figure 6: Lan Zhou city, suffering from a sandstorm. The visibility is only 300 m.

PM (particulate matter or fine particles) is defined as the amount of particles of solid or liquid matter suspended in a gas or liquid. PM_{10} refers to all particles which are no more than 10 μm in aerodynamic diameter. The length is about one-seventh the diameter of a human hair, PM_{10} includes both the coarse particulate matter (diameter of 2.5 μm to 10 μm) and the fine particulate matter (diameter less than 2.5 μm), $PM_{2.5}$. The coarse particulate matter is mostly produced in mechanical processes, while the fine particulate matter is mainly produced by fuel combustion. In most cities, these two kinds of particulates appear at the same time. However, the composition ratio may vary according to different geographical conditions, weather factors and the special pollution sources in different cities. The observed mean concentration of some aerosol particles in Lan Zhou city between the years 2005 - 2008 has been: SO_2: 0.0610 mg m^{-3}, NO_x: 0.066 mg m^{-3} PM_{10}: 0.431 mg m^{-3} and $PM_{2.5}$: 0.276 mg m^{-3} (Zhao, 2007).

Table 2 lists the recommended limits for PM_{10} and $PM_{2.5}$ by the European Union and Sweden. They can be used for comparison with the Chinese data.

Table 2: The recommended limits for PM_{10} and $PM_{2.5}$ in the EU and Sweden in 2005 (mg m^{-3}) (European Commission, Air Quality Standards, 2012), and as measured in Lan Zhou (Zhao, 2007).

Country	**Average (daily and monthly)**	**PM_{10}**	**$PM_{2.5}$**
Sweden	Daily	0.10	
	Annual	0.02	
EU	Daily	0.05	0.04*
	Annual	0.03	0.02
Lan Zhou	Measured mean in 2005-2008	0.431	0.276

*: no more than 14 times each year.

Table 2 shows that the observed mean PM_{10} and $PM_{2.5}$ concentrations in Lan Zhou were in 2005 - 2008 more than ten times the allowed annual limits in EU and Sweden.

The SACOL observations of aerosols in and around Lan Zhou (Sect. 2), along with observations in Europe, were used to create and validate the detailed aerosol model used in the LW radiation scheme of Sect. 3 (Eq. 14) (Wu, 1998; Zhao et al., 2005; Deng et al., 2010). The values of the key LW quantities, DLR, OLR and LHR, in conditions similar to those in Lan Zhou are shown in the tables of Sect. 4.3. The extreme case V = 0.3 km resembles the observed conditions during a strong sandstorm. The SACOL aerosol observations were used for model validation because they include both polluted urban and continental desert aerosol cases, they are carefully made, and they include some of the heaviest aerosol loads observed in the northern hemisphere.

2 Observations of aerosols in north western China and the city of Lan Zhou

The results of some of the spectral aircraft and tower observation campaigns of aerosol particles made at and around the SACOL stations of the University of Lan Zhou are presented here and compared with the assumptions made in Eq. 14, Sect. 1.1.3.2 for the aerosol extinction coefficient $\beta_{ae} = \beta_{ae}(\lambda,V,z)$.

2.1 The relationship between the aerosol optical depth and wavelength

The relationship between the column aerosol optical depth (AOD, τ_a) and the wavelength was investigated by Zhao et al. (2005). The results are summarized in Fig. 7. The data was collected in December 5th, 6th and 10th 1999 at the Lan Zhou University SACOL Yu Zhong observation station on the China Loess Plateau, 48 km from the city of Lan Zhou. The altitude of the Yu Zhong station is 1530 m, which is 620 m higher than the city. The weather at the time of the measurements was sunny and cloudless.

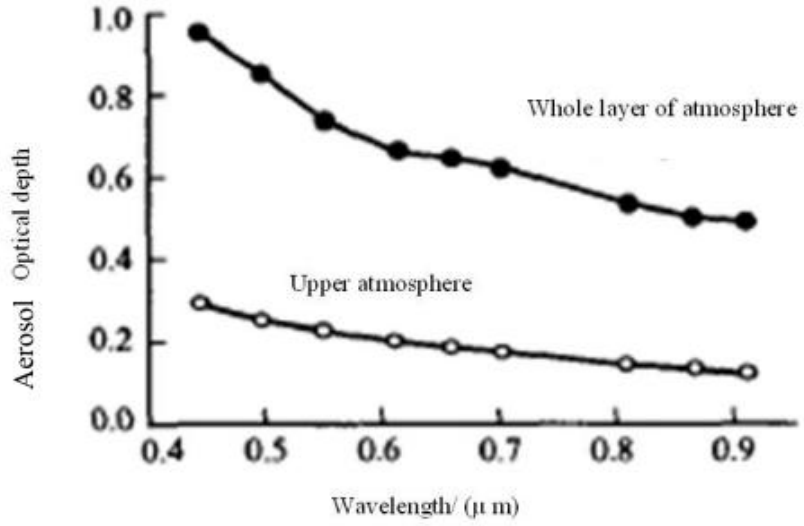

Figure 7: The aerosol optical depth τ_a as a function of wavelength (Zhao et al., 2005).

Fig. 7 shows that in the plateau region the AOD behaves as $\sim\lambda^{-1}$, especially near the surface. This agrees with the assumption made in Sect. 1.1.3.2 and Eq. 14. The AOD of the whole air column is about 0.75 at λ = 0.55 μm, indicating lots of mineral dust in the air at the time of the measurements.

2.2 Ångström turbidity parameter and wave length exponent

The Ångström turbidity parameter is an atmospheric optical parameter that represents the amount of aerosol particles in the atmosphere (not including clouds and fog). It is

often used as a measure of air pollution. In 1964, Ångström suggested the following equation for the aerosol optical depths:

$$\tau_{a,\lambda} = \beta\lambda^{-\alpha}, \tag{16}$$

where $\tau_{a,\lambda}$ is the AOD for the wavelength λ given in μm, β is the Ångström turbidity parameter and α is the wavelength exponent. In the literature β is usually given at the reference wavelength of 1 μm. The values of $\beta < 0.2$ are associated with clean air (Wu, 1998).

Fig. 8 shows the diurnal variation of α observed at the plateau from Zhao et al. (2005).

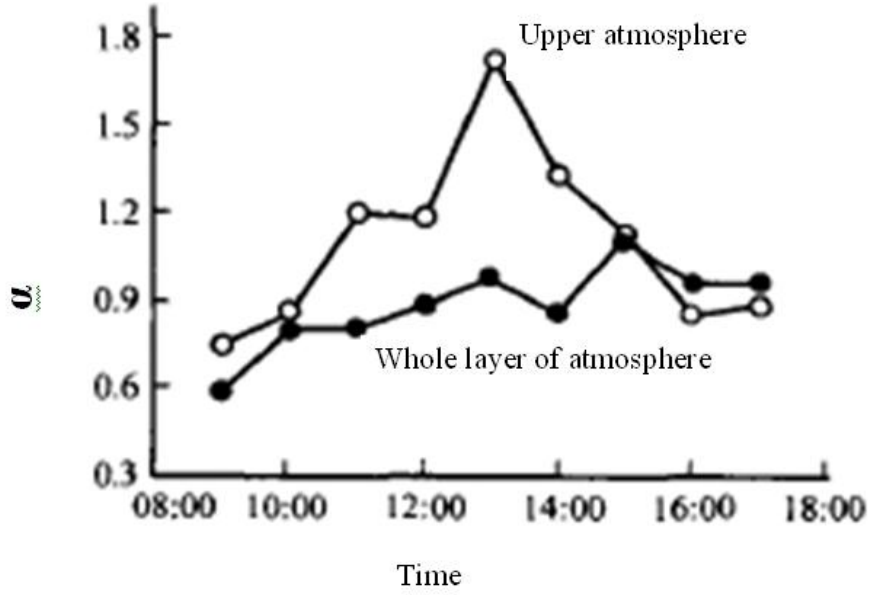

Figure 8: The diurnal variation of the Ångström wavelength exponent α in Lan Zhou (Zhao et al., 2005).

The data shows that $\alpha \approx 0.7\text{-}1.1$; $\alpha = 1$ was assumed for the aerosol volume extinction coefficient β_{ae} in Eq. 14.

2.3 Relationship between the aerosol optical depth and the meteorological visibility

The relationship between AOD and the meteorological visibility V was also investigated by Zhao et al (2005). The results are shown in Fig. 9.

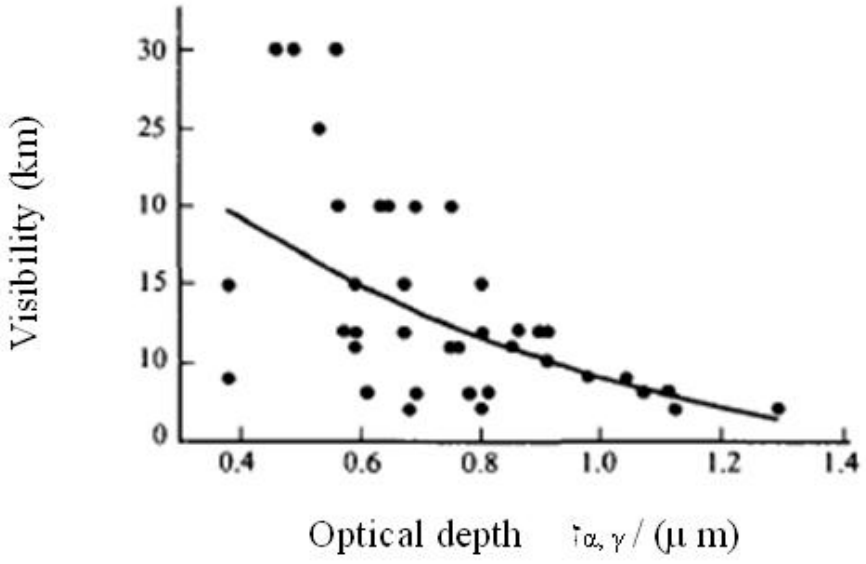

Figure 9: The results of the observations of meteorological visibility V and the optical depth τ_a during the Lan Zhou campaign (Zhao et al., 2005).

The (scattered) data of Fig. 10 indicates that $\tau_a \sim V^{-1}$ in the Lan Zhou region, especially for the highly polluted values of $\tau_a > 0.8$. This result agrees with the aerosol model described in Sect. 1.1.3.2 and Eq. 14. The observed average τ_a is ~0.75, which is in agreement with Fig. 7.

2.4 Aerosol volume extinction coefficient as a function of height

The relationship between the aerosol volume extinction coefficient β_{ae} and height z was investigated around Lan Zhou by Deng et al. (2010). The data was collected in October 22nd at Lan Zhou University roof (36.0541°N, 103.8586°E, altitude 1525 m). The weather at the time of the measurements was clear and the wind was light. Due to the light wind the aerosol pollution did not spread and dissipate efficiently and the effects of aerosol particles on the radiation were significant. The results are shown in Fig. 10.

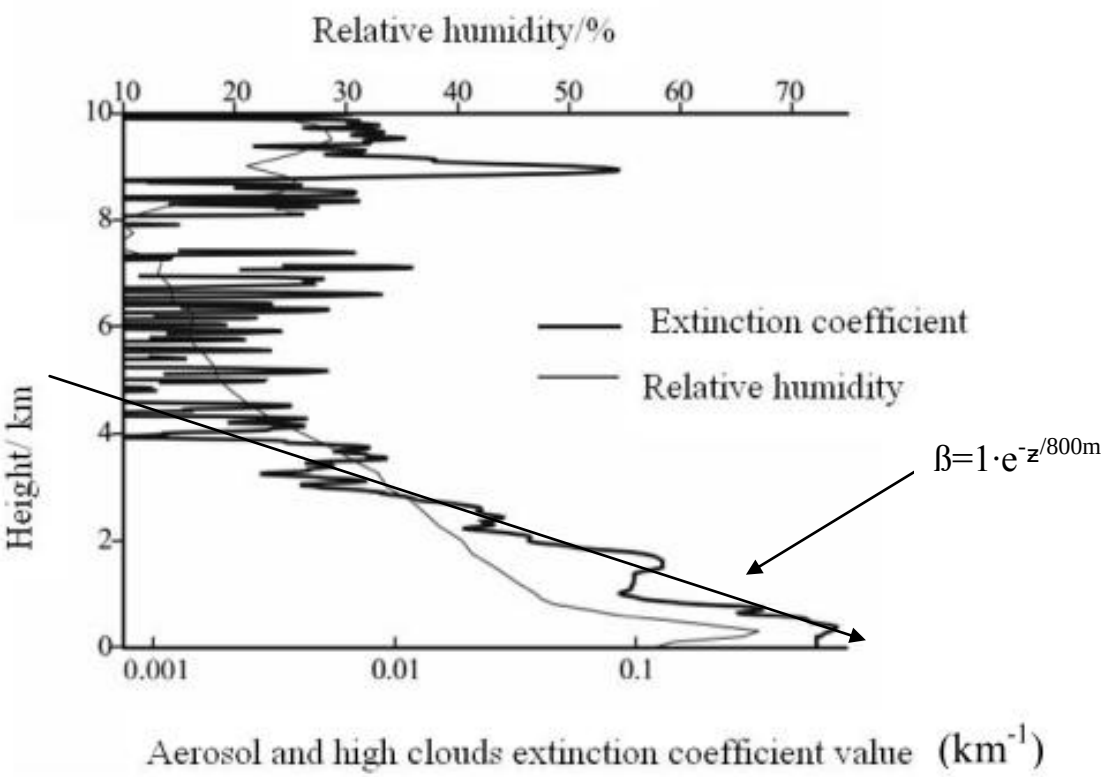

Figure 10: The measured profiles of aerosol (and high cloud) volume extinction coefficient β_{ae} and relative humidity (Deng et al., 2010).

From Fig. 10, one can see that below about 5 km

$$\beta_{ae} \sim e^{-z/H}, \tag{17}$$

where z is height and the scale height H of the exponential decay is about 800 m. The value 1 km for H was assumed in the aerosol model of Eq. 14. If β_{ae} is assumed to be $\beta_0 = 1$ km^{-1} at the surface, as indicated by Fig. 10, Eq. 3 and Eq. 14 give

$$\tau_a = \int_0^\infty \beta_{ae}\, dz = \beta_0 \int_0^\infty e^{-z/H} dz = -\beta_0 H \left(e^{-\infty} - e^0 \right) = \beta_0 H = 1 km^{-1} \cdot 1 km = 1$$

and the required visibility from Eq. 14 at $\lambda = 0.55$ μm at the surface (z = 0) then is 4 km. This model-produced value fits the independent visibility observations of Fig. 9 reasonably well.

3 The Long-Wave Radiation Scheme

The effect of aerosols on the LW greenhouse effect is the main subject of this study. This was analyzed by making LW calculations in a typical mid-latitude summer air column (MLS case of Ellingson et al., 1991) with a narrow-band spectral LW scheme (Savijärvi, 2006), which allows the modelling of variable aerosol, cloud, and greenhouse gas loads.

The LW radiation scheme (taken from (Savijärvi, 2006)) calculates the upwelling and downwelling LW fluxes (L_{up}, L_{down}) at each altitude from solutions to the plane-parallel equation of radiative transfer, using the nonscattering absorption approximation with a diffusivity factor of $1/\mu_1 = 1.66$ (Eq. 8), and assuming local thermodynamic equilibrium. Therefore the spectral fluxes at each wave number $k = 1/\lambda$ for a narrow band Δk around k are calculated with Eq. 9 and Eq. 10.

The main computational problem is how to represent the strong spectral variation of the transmissivities t_k for the millions of absorption/emission lines of the greenhouse gases in each air layer. A line-by line (LBL) calculation would be far too slow in an interactive model. Therefore a statistical narrow-band model (NBM) for the gaseous transmissivity $t_{gas,k}$ was adopted. The NBM covers the $0 - 1200\ \mathrm{cm}^{-1}$ wave number range in 48 bands ($\Delta k = 25\ \mathrm{cm}^{-1}$), the $1200 - 2100\ \mathrm{cm}^{-1}$ range in 18 bands ($\Delta k = 50\ \mathrm{cm}^{-1}$), and the $2100 - 2500\ \mathrm{cm}^{-1}$ range in one band; so there are 67 bands in the LW range. The band parameters for water vapour, CO_2 and O_3 were taken from Houghton (2002). The Goody random band model was adopted for water vapour, the Malkmus model for CO_2 and O_3, and the Curtis-Godson method was used for line pressure broadening along inhomogeneous vertical paths. The Roberts scheme (Roberts et al., 1976), augmented with foreign-broadened contribution, was considered sufficient for the very important water-vapour continuum effect in the present study, which concentrates mainly on the boundary layer aerosol effects, although the more comprehensive Clough continuum scheme (Clough et al., 1992) is recommended for studies that would concentrate on the upper troposphere and higher altitudes.

The local LW heating rate (LHR) of air is obtained as the vertical convergence of the total net LW flux $L_{net} = L_{up} - L_{down}$. Thus at each height z, LHR is given by Eq. 12.

The NBM should be validated before using it for aerosol-laden atmospheres. This was done in Savijärvi (2006), where the key LW flux values were compared with results from the International Comparison of Radiation Codes in Climate Models (ICRCCM) for the mean mid-latitude summer input profiles for temperature, water vapor and O_3 (Ellingson et al., 1991), and also with values obtained using the Clough LBL model (Clough et al., 1992) with their continuum. These comparisons (Table 3) show that the present NBM is within the narrow range of the LBL results, and is very close to the 35-model all-gases median of ICRCCM. Thus the clear sky reference MLS case without aerosols is well simulated by the present LW NBM.

Table 3: Comparison of the present NBM results, Clough et al. (1992) LBL model and the ICRCCM results for the mean MLS input profiles for temperature, water vapor and O_3 (Ellingson et al., 1991) (From Savijärvi, 2006).

TABLE 1. DOWNWELLING AND UPWELLING LONG-WAVE FLUXES (W m^{-2})

Midlatitude summer profiles (ICRCCM, Ellingson *et al.* 1991)	Surface down	Tropopause up	Tropopause down
Water-vapour lines only:			
ICRCCM LBL range (three models)	266–268		
Clough *et al.* LBL (1992)	269.0	335.8	6.9
Present NBM	266.8	333.0	6.3
Water vapour with continuum:			
LBL range (three models)	320–330		
Clough *et al.* LBL (1992)	333.8	321.3	7.4
Present NBM	324.0	326.4	7.4
All gases active:			
LBL range (three models)	340–345		
ICRCCM median (35 models)	343.4	291.2	22.1
Present NBM	344.9	291.0	22.4

ICRCCM midlatitude summer atmosphere with 300 ppmv of CO_2. Surface emissivity is 1.0 and the upwelling flux at the surface is 423.62 W m^{-2}. LBL is line-by-line and NBM is narrow-band model representation; see text for further details.

The typical upward increase of the net LW flux produces LW cooling (Eq. 12), which amounts to LHR ~ -1.74 K day^{-1} on the average for the whole MLS atmospheric column. For the MLS troposphere only, using the flux values from table 3, one obtains LHR ~ -1.86 K day^{-1}.

3.1 Aerosols in the LW Scheme

Aerosols were added to the above spectral NBM scheme by assuming their typical schematic observed behaviour over European land areas and around the city of Lan Zhou (Sect. 2). The aerosol volume extinction coefficient β_{ae} (km^{-1}) is hence assumed to depend on the meteorological visibility V, wavelength λ and height z according to Eq. 14. The aerosol vertical optical depth (AOD; τ) is calculated from β_{ae} with Eq. 3 for each layer and each band. Assuming no scattering (a good approximation in the LW range) the LW diffuse transmissivity of aerosols t_a is obtained from Eq. 8 and the total transmissivity for each layer and each band is obtained by combining the transmissivities for the greenhouse gases and aerosols according to Eq. 15. The LW fluxes are then calculated using Eqs. 9 and 10.

4 Results

4.1 Reference case: clear sky MLS with 300 ppm of CO_2

The clear sky mean mid-latitude summer (MLS) case of the International Comparison of Radiation Codes in Climate Models, with 300 ppm of CO_2 and no aerosols/clouds was used as the reference case. The main MLS input variables are *T(z)* and *q(z)*, where T is the temperature and q the water vapour mixing ratio. The temperature profile is shown graphically in Fig. 11. The ozone profile and *q(z)* are given in Ellingson et al. (1991). The LW scheme output, i.e. the clear-sky downward and upward fluxes, the net flux (all in W m^{-2}), and the LW heating rate (K day^{-1}) (Eq. 12), are shown in Figures 12 and 13.

At the model top (104 km), the OLR is 287.57 W m^{-2}. At the surface the DLR is 344.76 W m^{-2} and the upward flux is 423.62 W m^{-2}. (The ground emissivity is assumed to be 1, which corresponds to the blackbody emission, σT^4, of the surface (at 294 K). The net flux difference is therefore 78.85 W m^{-2} at the surface. The net flux increases upward (Fig. 3), its gradient giving the local LW heating rate, LHR (Eq. 12). LHR is about -3.8 K day^{-1} near the surface and about -2 K day^{-1} in the upper troposphere, as shown in Fig. 13.

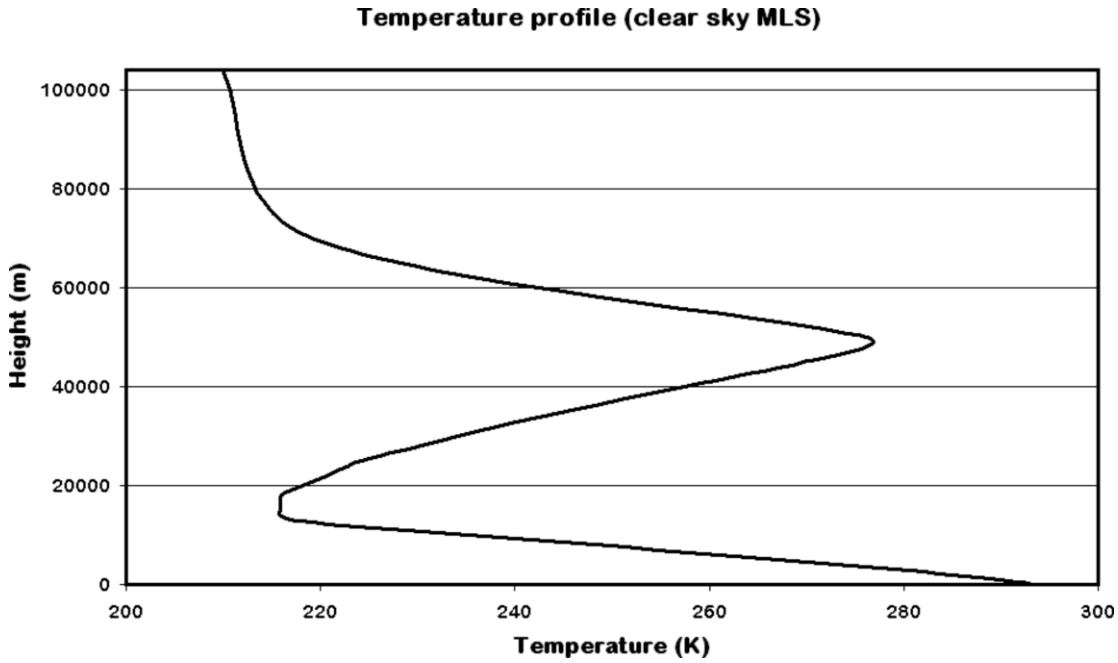

Figure 11: The MLS temperature profile used as an input variable for the LW scheme.

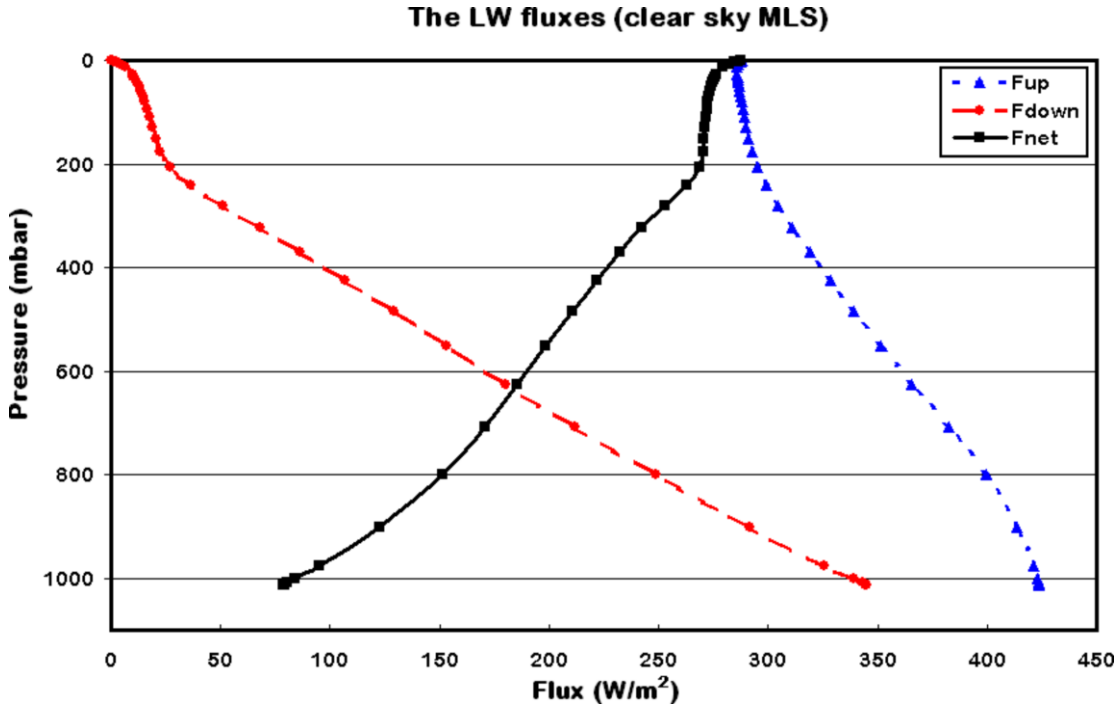

Figure 12: The NBM scheme LW fluxes in the clear sky MLS case without aerosol.

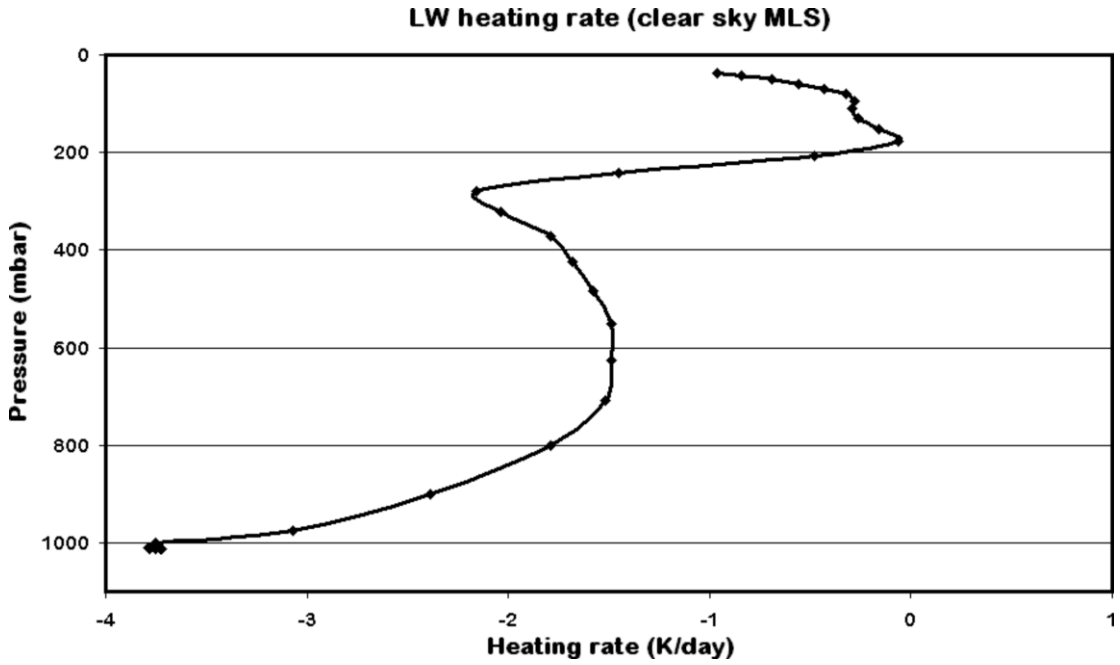

Figure 13: The local LW heating rate in the clear sky MLS case without aerosol.

4.2 Effect of aerosols on LW fluxes

The NBM model was now applied at the reference MLS case, but using various amounts and profiles of clouds, CO_2 and aerosols in order to better understand the factors changing the key LW quantities DLR, OLR and LHR from the clear-sky case.

The cloud effects were first studied, by varying the low cloud (1-2 km) liquid water vertical path (LWP) in the NBM model. The cloud effects as estimated from global annual satellite measurements were shown in table 1. The NBM model MLS case results are listed in table 4 below.

Table 4: The relationship between low cloud LWP and the key LW quantities.
LWP = 0 is the clear sky reference. LHR is the mean LHR for the whole column.

Low cloud (1 - 2 km) LWP, g/m^2	DLR W/m^2	OLR W/m^2	LHR K/day
0 (= no cloud)	**344.76**	**287.57**	**-1.739**
1	353.51	286.38	-1.802
10	393.53	280.93	-2.091
100	407.53	279.03	-2.191
300	407.53	279.03	-2.191

From table 4 one can see that a thick low cloud will lead to a strong increase in the DLR and to a decrease in the OLR, the latter in agreement with the satellite measurements (satellites cannot measure the DLR). Further, the thick low cloud will also lead to the increase of the column longwave cooling rate. A thick cloud with LWP > 100 g/m^2 behaves like a blackbody, so the values do not change from the values of the last line for LWP > 300 g/m^2.

The effect of the CO_2 concentration on the LW quantities was also studied. According to the NBM model applied on the clear-sky MLS case, the increase of the CO_2 concentration from 300 ppm to 600 ppm increases the DLR by about 2 W m^{-2}, while the OLR decreases by about 2.2 W m^{-2}. This results in a minor increase of the LHR from -1.739 K/day to -1.737 K/day. These values are in good agreement with the estimated global mean radiative forcing effect due to doubled CO_2.

The NBM model was first applied to the effects of aerosols on the LW quantities by studying the influence of a heavy aerosol load in the lower stratosphere. An aerosol layer with constant β_{ae} = 0.1 km^{-1} at 0.55 μm was added to the MLS case between 14 – 24 km. The AOD of this 10 km deep layer is hence 1. Such a heavy aerosol load could be produced by a major volcanic eruption. The results show that the heavy volcanic aerosol load in the stratosphere will increase the DLR slightly, and decrease the OLR moderately. The DLR increase was 1.71 W m^{-2} and the OLR decrease

20.58 W m^{-2}. As the volcanic dust layer net absorbs the surface emission, there is also a 0.157 K/day decrease in the LW cooling rate, compared to the clear-sky case.

Tropospheric aerosols were modelled using two different approaches, and the results were compared. The first assumes a vertically constant low-level aerosol volume extinction coefficient β_{ae} (km^{-1}) to some height, and the second approach assumes an exponentially decaying aerosol load (Eq. 14). The NBM results with constant β_{ae} are listed in table 5.

Table 5: LW quantities with aerosol layers of different height assuming a vertically constant low-level aerosol volume extinction coefficient β_{ae} = 0.1 km^{-1} at 0.55 μm.

Aerosol layer km	τ_{vis}	DLR W/m^2	OLR W/m^2	LHR K/day
0	**0**	**344.76**	**287.57**	**-1.739**
0-1	0.15	346.41	287.47	-1.752
0-2	0.25	347.35	287.25	-1.758
0-3	0.35	348.17	286.87	-1.762

The results in table 5 show that a vertically constant dust layer with $\tau > 0.2$ already increases the DLR more than the doubled CO_2 did. On the other hand the near-surface dust load has a lesser effect on the outgoing long-wave radiation at the top of the atmosphere than the doubled CO_2 concentration. Assumption of constant β_{ae} with height is, however, often less realistic than the exponentially decaying dust load. Table 6 therefore shows results for the exponentially decaying aerosol model (Eq. 14) as the function of visibility, with the scale height H fixed to 1 km.

Table 6: The relationship between the horizontal meteorological visibility V and the LW quantities according to the the aerosol LW model (eq. 14) in the MLS case.

V Km	τ_{vis}	DLR W/m^2	OLR W/m^2	LHR K/day
∞	**0**	**344.76**	**287.57**	**-1.739**
50	0.08	345.67	287.48	-1.746
20	0.20	347.00	287.34	-1.756
10	0.40	349.15	287.11	-1.772
1	4.00	377.97	283.53	-1.982
0.3	**13.33**	**406.87**	**277.26**	**-2.171**

The results listed in table 6 show that the typical "good visibility" case of V = 20 km ($\tau_{vis} \sim 0.2$) corresponds to the DLR increase of 2.24 W m^{-2} and the OLR decrease of only 0.23 W m^{-2} from the clear sky reference case (the top line). The values of the LW quantities obtained with the two different approaches for $\beta_{ae}(z)$ agree quite well for the same AOD, τ_{vis}.

The lowest row of Table 6, an extreme case of a really low visibility, V = 300 m, represents conditions during a heavy dust storm, such as illustrated in Fig. 6. It indicates an extremely high AOD, $\tau_{vis} \sim 13$. **The effect of such a heavy dust storm is according to Table 6 similar to that of a thick low cloud with LWP ~ 100 g m^{-2} (Table 4).** The DLR increase from the clear sky case is a whopping 62 W m^{-2} and the OLR decrease, 10 W m^{-2}.

The relationship between the visibility and the LW quantities was further investigated by varying the scale height H in Eq. 2. The visibility was fixed to the nominal V = 20 km. The results are shown in table 7.

Table 7: The relationship between the visibility, scale height *H* and the LW quantities for the aerosol LW model (Eq. 2).

H m	*V* km	τ_{vis}	DLR W/m2	OLR W/m2	LHR K/day
500	20	0.11	346.02	287.52	-1.749
800	20	0.17	346.62	287.43	-1.754
1000	**20**	**0.21**	**347.00**	**287.34**	**-1.756**
2000	20	0.41	348.64	286.51	-1.763
800	**4**	**0.85**	**353.55**	**286.87**	**-1.807**

The results of table 7 show that the increase of the scale height *H* from 500 m to 2 km increases the AOD from $\tau_{vis} = 0.1$ to $\tau_{vis} = 0.4$. The DLR increases by 2.62 W m^{-2} and OLR decreases by 1.01 W m^{-2}. This results in the LW cooling decreasing from -1.749 K/day to -1.763 K/day.

The visibility $V = 4$ km and the scale height $H = 800$ m corresponded to the average (not extreme) observed conditions in the city of Lan Zhou during heavy industrial aerosol loads (see Figs 9-10). The AOD is ~ 0.85. According to the NBM model, the DLR would be in such polluted conditions 353.55 W m^{-2}, and OLR, 286.87 W m^{-2}. The LHR would decrease to -1.807 K/day. Comparison of these values with those of a low cloud in table 4 reveals that **the impact heavy (but not extreme) man-made aerosol load on the LW quantities is similar to that of a thin low cloud with a LWP of about 1 g m^{-2}**.

The combined effects of aerosols and low clouds were next investigated by adding an aerosol layer (0 – 1 km) with constant β_{ae} under a thin low cloud at 1 - 2 km. The LW quantities with different values of β_{ae} are shown in table 8.

Table 8: The LW quantities with a thin low cloud (LWP = 1 g m^{-2}) at 1 - 2 km and aerosol layer with constant β_{ae} set below it at 0 – 1 km.

Aerosol amount at 0-1 km β_{ae}, km^{-1}	DLR W/m^2	OLR W/m^2	LHR K/day
0	353.51	286.38	-1.802
0.001	353.52	286.38	-1.802
0.01	353.65	286.37	-1.803
0.1	354.94	286.29	-1.814
0.3	357.71	286.11	-1.835
1	366.39	285.52	-1.903

The values of table 8 show that **thick aerosol below a thin low cloud results in a moderate increase of DLR and the longwave cooling rate, but only a small decrease of OLR,** as the cloud top outradiation dominates the OLR.

The effect of an aerosol layer on the local LW fluxes and the local LW heating rate was also investigated. Constant $\beta_{ae} = 0.1$ km^{-1} at 0.55 μm was used for the near-surface aerosol cases. The clear sky MLS case with 300 ppm of CO_2 was used as a reference, and only the deviations from it are shown.

The effect of these well-mixed aerosols to the LW fluxes in the MLS air column is shown in Fig. 14, which displays the LW net flux deviations from the clear sky reference case values (Fig. 12) as a function of air pressure and the layer thickness.

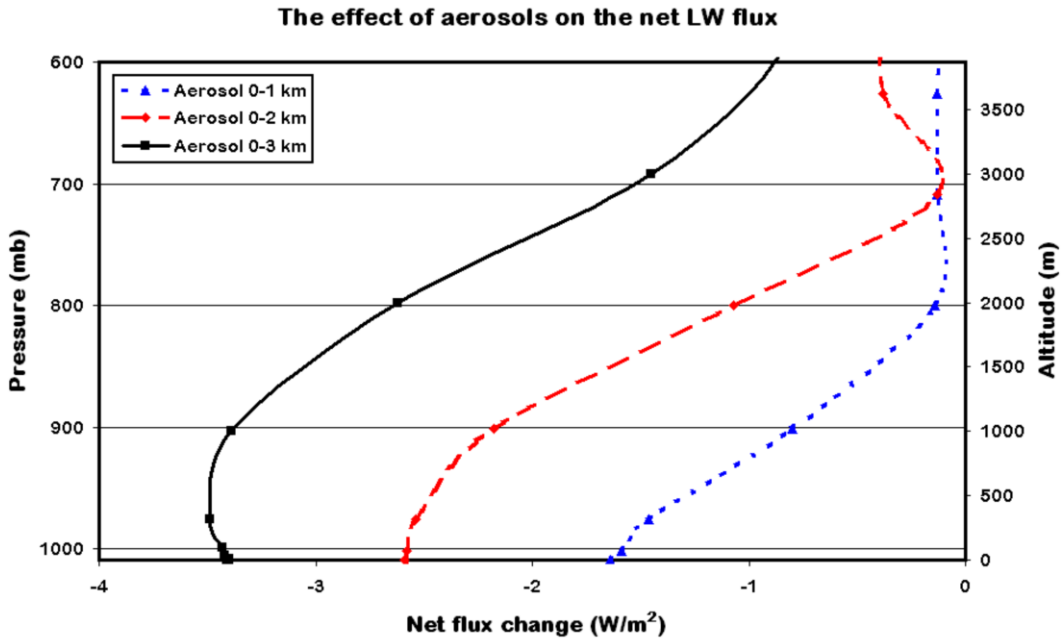

Figure 14: The effect of aerosols on the net LW flux of the MLS case. Vertically constant β_{ae} of 0.1 km^{-1} at 0.55 μm ("well-mixed aerosol").

Fig. 6 shows that the aerosols act to decrease the net flux from the clear sky value near the top of the current aerosol layer. With fixed β_{ae}, the strength of the effect depends on the thickness of the layer, and for a thick layer the decrease gets smaller near the surface.

The net flux gradient yields the local LW heating rate by Eq. 12. The deviations of the local LW heating rate from the clear sky case (Fig. 13) are shown in Fig. 15.

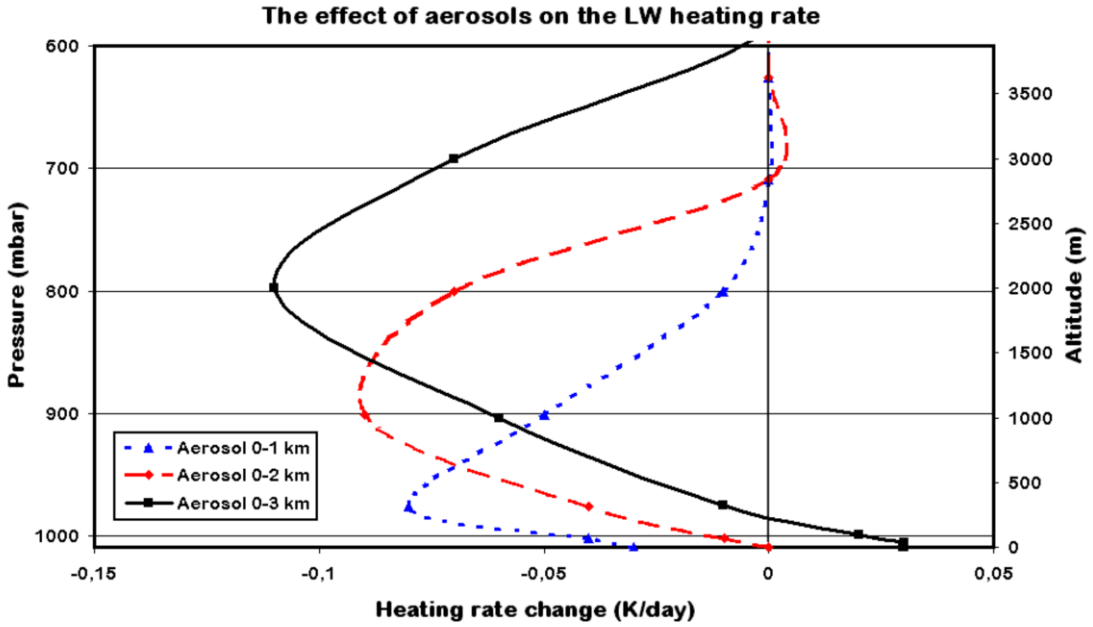

Figure 15: The effect of aerosols on the LW heating rate of the MLS case. Vertically constant β_{ae} of 0.1 km^{-1} at 0.55 µm ("well-mixed aerosol").

Fig. 15 shows that the clear-sky LW heating rate decreases within the aerosol layer, and the strength of the decrease depends on the thickness of the layer. **The extra local LW cooling caused by aerosols is strongest in the middle of each aerosol layer (of constant concentration).** The LW heating rates above the top of the aerosol layer and near the surface are affected only slightly. An aerosol layer of less than 0 – 2 km appears to have a small cooling effect very near the surface, while a thicker layer displays a slight warming effect.

Fig. 16 displays how an exponentially decaying aerosol load affects the net LW flux of the MLS air column. The β_{ae} was calculated from the horizontal meteorological visibility V by Eq. 14. Scale height H was set to 1 km. The corresponding total LW heating rates are given by Eq. 12. The deviations of these LW heating rates from the clear sky MLS case are shown in Fig. 17.

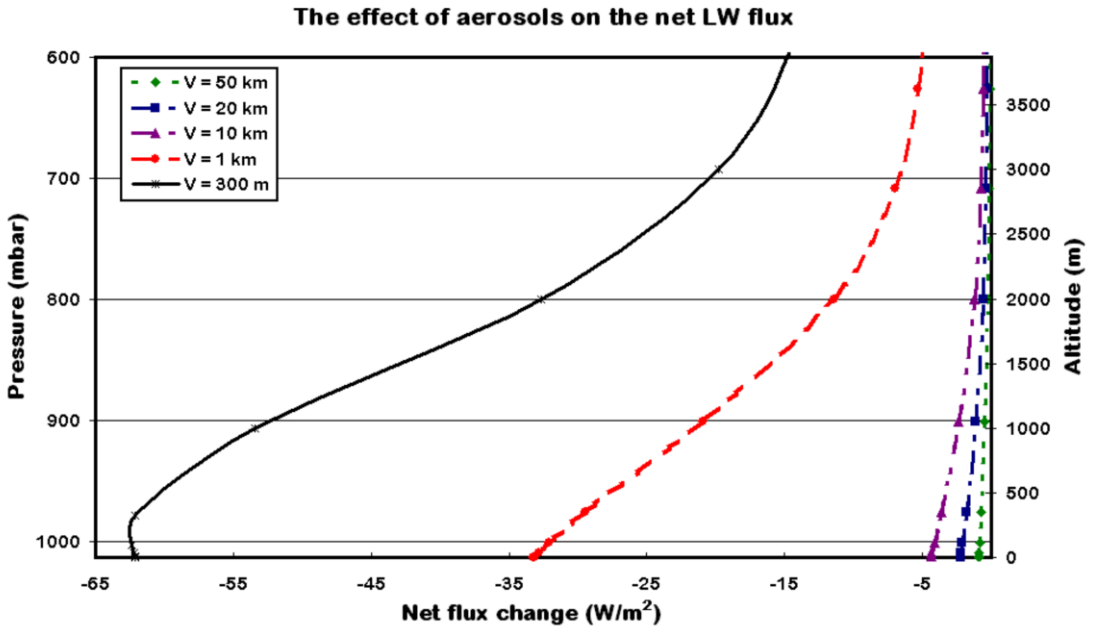

Figure 16: The effect of aerosols on the net LW flux of the MLS case as a function of pressure and meteorological visibility *V*. Aerosol load was assumed to decay exponentially with scale height H = 1 km.

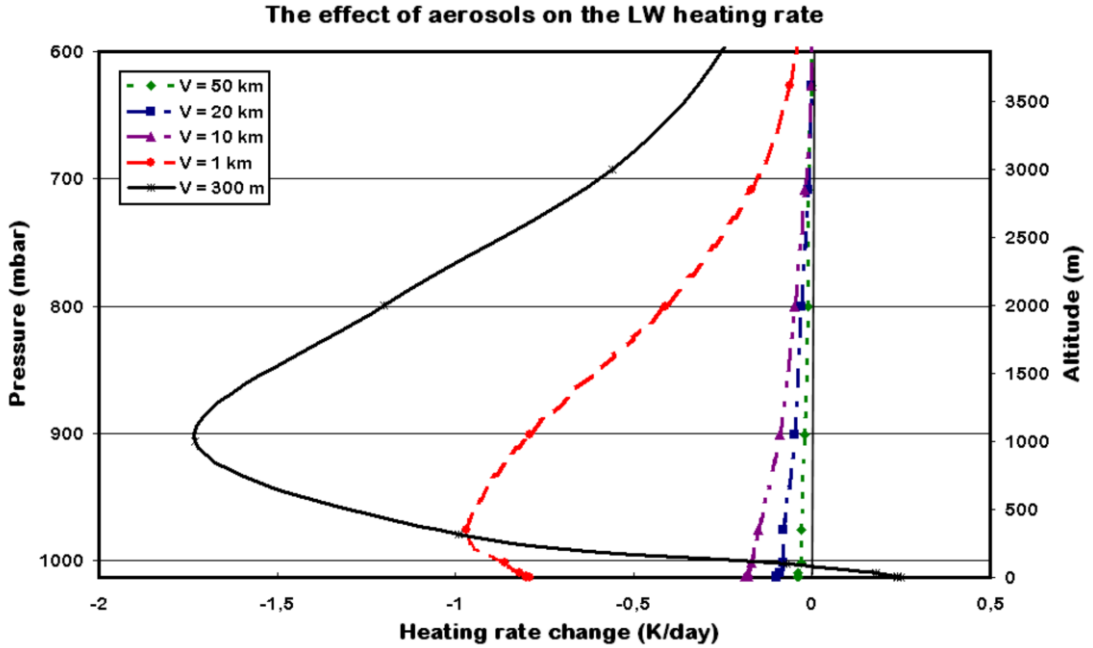

Figure 17: The effect of aerosols on the LW heating rate of the MLS case. Aerosol load was assumed to decay exponentially with scale height H = 1 km.

Comparing Figs. 14 – 17 and Tables 5 and 6, one can see that the results obtained assuming constant β_{ae} and an exponentially decaying aerosol are slightly different. The effect of exponentially decaying aerosol load on the net flux does not decrease near the surface (as was the case with constant β_{ae}), unless the aerosol concentration is extremely high. As a consequence, **the LW cooling effect is always strongest near the surface for light to moderate exponentially upward decaying aerosol loads**. The aerosol concentration must be extremely high for it to have a warming effect very near the surface.

5 Conclusion

The effect of aerosols on the LW radiation was studied with a LW radiation scheme using a narrowband model for the gaseous absorption and emission of radiation. Aerosols were added to this model by assuming their typical properties via Eq. (14) according to observations in Europe and those made recently in north-western China, as reviewed briefly in Section 2. The ICRCCM mid-latitude summer atmosphere (MLS) with 300 ppm of CO_2 was used as a reference case. The impact of aerosols was then studied by adding or varying the amounts of low cloud, CO_2 and aerosols in the MLS case. The quite heavy natural sandstorm and man-made average industrial aerosol loads as observed in and near the city of Lan Zhou in NW China were used as examples.

The results confirm the hypothesis that an aerosol layer has a similar general effect on the LW quantities at all heights as a thin cloud, absorbing the LW radiation from air and surface, and re-emitting partially back towards the ground. The general result is hence an increase in the downwelling longwave radiation at the surface and a slight decrease in the outgoing LW radiation. Adding near-surface aerosol or a low cloud, both lead to an increased column LW cooling rate. However, adding extra CO_2 or a stratospheric aerosol layer does decrease the overall LW cooling rate.

The local effect of aerosols was studied by comparing the local net LW fluxes and the local heating rates of the aerosol cases to those of the clear sky reference case. The results show that the LW cooling rate increases from the clear sky case within a

near-surface aerosol layer. The strength of the effect depends on the height (thickness) of a well-mixed constant concentration aerosol layer. Locally, the cooling effect is then strongest in the middle of the layer and weaker at its top and near the surface. The cooling at the bottom of a shallow aerosol layer is slightly stronger than in the clear sky case, whereas a high and heavy well-mixed near-surface aerosol can lead to a warming effect very near the surface, like a low cloud or fog does. A cold stratospheric aerosol layer leads on the other hand to local LW warming, again like a thin high (cirrus ice) cloud does, as the cold layer net absorbs the emission from the much warmer surface.

The strength of the effect of aerosols depends also on the profile of the aerosol concentration, which is often highest very near the surface with an exponential decay upwards. Here the LW cooling effect is usually stronger near the surface than near the top of the layer, where the aerosol concentration is lower. In practice, for near-surface aerosols to cause local LW warming near the surface, the concentration has to be extremely high; sand storm-like.

These quantitative estimates of the so far small aerosol LW effect to the climate are becoming relevant, as the industrial loading of aerosol is rapidly increasing in many large cities, particularly in South-East Asia, where even regional effects are already probable.

References

Claquin, T., Schulz, M., Balkanski, Y., 1997. A modeling study of the shortwave and longwave forcing by dust aerosols. J.Aerosol Sci. 28, 447-448.

Clough, S.A., Iacono, M.J., Moncet, J.L., 1992. Line-by-line calculations of atmospheric fluxes and cooling rates: Application to water vapour. J.Geophys.Res. 97(D14), 15761–15785.

Dammann, K.W., Hollmann, R., Stuhlmann, R., 2000. Study of aerosol impact on the earth radiation budget with satellite data. Adv. Space Res. 29, 1753-1757.

DeLiberty, T., 1999. Energy interactions with the atmosphere at the surface (cited March 9th, 2014) www.udel.edu/Geography/DeLiberty/Geog474/geog474_energy_interact.html

Deng, T., Zhang, L., Wu, D., Xia, J.L., Song, W., Deng, X.J., Tan, H.B., Bi, X.Y., Li, F., 2010. The high cloud and aerosol optical properties, as well as their radiative effects in Lan Zhou area. Plateau Meteorol.J. 29, 230-235.

Ellingson, R.G., Ellis, J., Fels, S.B., 1991. The intercomparison of radiation codes used in climate models: Long wave results. J.Geophys.Res. 96(D5), 8929–8953.

Greenhouse effect (cited July 30th 2011), http://environment-clean-generations.blogspot.com/2011/07/greenhouse-effect.html

Hartmann, D.L., 1994. Global Physical Climatology. Academic Press, New York.

Han, Z., Li, J., Xia, X., Zhang, R., 2012. Investigation of direct radiative effects of aerosols in dust storm season over East Asia with an online coupled regional climate chemistry-aerosol model. Atmos.Environ. 54, 688-699.

Houghton, J.T., 2002. The physics of atmospheres, 3rd ed. Cambridge University Press, Cambridge.

Lenoble, J., 1986. Detection of stratospheric aerosol characteristics in relation with climate impact. Adv.Space Res. 6, 63-72.

European Commission, Air Quality Standards (cited April 6th 2012), http://ec.europa.eu/environment/air/quality/standards.htm

Meehl, G.A., T.F. Stocker, W.D. Collins, P. Friedlingstein, A.T. Gaye, J.M. Gregory, A. Kitoh, R. Knutti, J.M. Murphy, A. Noda, S.C.B. Raper, I.G. Watterson, A.J. Weaver and Z.-C. Zhao, 2007 Global Climate Projections. Climate Change 2007: The Physical Science Basis. Contribution of Working Group I to the Fourth Assessment Report of the Intergovernmental Panel on Climate Change, Cambridge University Press, Cambridge, United Kingdom and New York, NY, USA

Method, T.J., Carlson, T.N., 1982. Radiative heating rates and some optical properties of the St. Louis aerosol, as inferred from aircraft measurements. Atmos.Environ. 16, 53-66.

Mickley, L.J., Leibensperger, E.M., Jacob, D.J., Rind, D., 2012. Regional warming from aerosol removal over the United States: Results from a transient 2010–2050 climate simulation. Atmos.Environ. 46, 545-553.

Péré, J.C., Colette, A., Dubuisson, P., Bessagnet, B., Mallet, M., Pont, V., 2012. Impacts of future air pollution mitigation strategies on the aerosol direct radiative forcing over Europe. Atmos.Environ. 62, 451-460.

Paltridge, G.W., Platt, C.M.R., 1976. Radiative processes in meteorology and climatology. Elsevier, Amsterdam.

Reck, R.A., 1975. Influence of aerosol cloud height on the change in the atmospheric radiation balance due to aerosols. Atmos.Environ. 9, 89-99.

Ramachandran, S., Kedia, S., 2011. Aerosol radiative effects over an urban location and a remote site in western India: Seasonal variability. Atmos.Environ. 45, 7415-7422.

Roberts, R.E., Selby, J.A., Biberman, L.M., 1976. Infrared continuum absorption by atmospheric water vapour in the 8–12 μm window. Appl.Opt. 15, 2085-2090.

Savijärvi, H., 2006. Radiative and turbule 564 nt heating rates in the clear-air boundary layer. Q.J.R.Meteorol.Soc. 132, 147–161.

Savijärvi, H., Jin, L., 2001. Local winds in a valley city. Boundary-Layer Meteorol. 100, 301–319.

Shaocai, Y., Charles, S., Zender, S., Saxena, V.K., 2001. Direct radiative forcing and atmospheric absorption by boundary layer aerosols in the southeastern US: model estimates on the basis of new observations. Atmos.Environ. 35, 3967-3977.

South Daily News: Lan Zhou city, suffering from a sandstorm. The visibility is only 300 m. (cited March 21st 2010)(translated from Chinese), http://nf.nfdaily.cn/nfrb/content/2010-03/20/content_10286700.htm

Verma, S., Boucher, O., Upadhyaya, H.C., Sharma, O.P., 2006. Sulfate aerosols forcing: An estimate using a three-dimensional interactive chemistry scheme. Atmos.Environ. 40, 7953-7962.

Wendisch, M., Hellmuth, O., Ansmann, A., Heintzenberg, J., Engelmann, R., Althausen, D., Eichler, H., Müller, D., Hu, M., Zhang, Y., Mao, J., 2008. Radiative and dynamic effects of absorbing aerosol particles over the Pearl River Delta, China. Atmos.Environ. 42, 6405-6416.

Wu, B.Y., 1998. The practical algorithm of atmospheric radiative transfer. Meteorological Press, China.

Zhang, H., Shen, Z., Wei, X., Zhang, M., Li, Z., 2012. Comparison of optical properties of nitrate and sulfate aerosol and the direct radiative forcing due to nitrate in China. Atmos.Res. 113, 113-125.

Zhao, X.J., Chen, C.H., Yuan, T., Zhang, W., Dong, X.J., 2005. The relationship between atmospheric aerosol optical thickness and its visibility in the winter of Lan Zhou city. Plateau Meteorol.J. 4, 617-622.

Zhao, Q., 2007. The sources and control of the PM10 in the city. Southwest Normal University Press, China.

Appendix A

LW radiation scheme input data for the clear sky, stratospheric aerosol, doubled CO_2 and constant β_{ae} cases

Height	clear sky	stratospheric	CO2 300ppm -600ppm	aerosol 0-1km	aerosol 0-2 km	aerosol 0-3km
1	0.00	0.00	0.00	0.00	0.00	0.00
2	0.10	0.10	0.10	0.10	0.10	0.10
3	0.32	0.32	0.32	0.32	0.32	0.32
4	1.00	1.00	1.00	1.00	1.00	1.00
5	3.20	3.20	3.20	3.20	3.20	3.20
6	10.00	10.00	10.00	10.00	10.00	10.00
7	32.00	32.00	32.00	32.00	32.00	32.00
8	100.00	100.00	100.00	100.00	100.00	100.00
9	320.00	320.00	320.00	320.00	320.00	320.00
10	1000.00	1000.00	1000.00	1000.00	1000.00	1000.00
11	2000.00	2000.00	2000.00	2000.00	2000.00	2000.00
12	3000.00	3000.00	3000.00	3000.00	3000.00	3000.00
13	4000.00	4000.00	4000.00	4000.00	4000.00	4000.00
14	5000.00	5000.00	5000.00	5000.00	5000.00	5000.00
15	6000.00	6000.00	6000.00	6000.00	6000.00	6000.00
16	7000.00	7000.00	7000.00	7000.00	7000.00	7000.00
17	8000.00	8000.00	8000.00	8000.00	8000.00	8000.00
18	9000.00	9000.00	9000.00	9000.00	9000.00	9000.00
19	10000.00	10000.00	10000.00	10000.00	10000.00	10000.00
20	11000.00	11000.00	11000.00	11000.00	11000.00	11000.00
21	12000.00	12000.00	12000.00	12000.00	12000.00	12000.00
22	13000.00	13000.00	13000.00	13000.00	13000.00	13000.00
23	14000.00	14000.00	14000.00	14000.00	14000.00	14000.00
24	15000.00	15000.00	15000.00	15000.00	15000.00	15000.00
25	16000.00	16000.00	16000.00	16000.00	16000.00	16000.00
26	17000.00	17000.00	17000.00	17000.00	17000.00	17000.00
27	18000.00	18000.00	18000.00	18000.00	18000.00	18000.00
28	19000.00	19000.00	19000.00	19000.00	19000.00	19000.00
29	20000.00	20000.00	20000.00	20000.00	20000.00	20000.00
30	21000.00	21000.00	21000.00	21000.00	21000.00	21000.00
31	22000.00	22000.00	22000.00	22000.00	22000.00	22000.00
32	23000.00	23000.00	23000.00	23000.00	23000.00	23000.00
33	24000.00	24000.00	24000.00	24000.00	24000.00	24000.00
34	25000.00	25000.00	25000.00	25000.00	25000.00	25000.00
35	30000.00	30000.00	30000.00	30000.00	30000.00	30000.00
36	35000.00	35000.00	35000.00	35000.00	35000.00	35000.00
37	40000.00	40000.00	40000.00	40000.00	40000.00	40000.00
38	45000.00	45000.00	45000.00	45000.00	45000.00	45000.00
39	50000.00	50000.00	50000.00	50000.00	50000.00	50000.00
40	70000.00	70000.00	70000.00	70000.00	70000.00	70000.00
41	104000.00	104000.00	104000.00	104000.00	104000.00	104000.00

Pressure (mb)

clear sky	stratospheric	CO2 300ppm -600ppm	aerosol 0-1km	aerosol 0-2 km	aerosol 0-3km
1013.00	1013.00	1013.00	1013.00	1013.00	1013.00
1012.99	1012.99	1012.99	1012.99	1012.99	1012.99
1012.96	1012.96	1012.96	1012.96	1012.96	1012.96
1012.88	1012.88	1012.88	1012.88	1012.88	1012.88
1012.62	1012.62	1012.62	1012.62	1012.62	1012.62
1011.82	1011.82	1011.82	1011.82	1011.82	1011.82
1009.24	1009.24	1009.24	1009.24	1009.24	1009.24
1001.29	1001.29	1001.29	1001.29	1001.29	1001.29
975.94	975.94	975.94	975.94	975.94	975.94
901.13	901.13	901.13	901.13	901.13	901.13
800.15	800.15	800.15	800.15	800.15	800.15
708.84	708.84	708.84	708.84	708.84	708.84
626.30	626.30	626.30	626.30	626.30	626.30
551.86	551.86	551.86	551.86	551.86	551.86
484.88	484.88	484.88	484.88	484.88	484.88
424.70	424.70	424.70	424.70	424.70	424.70
370.73	370.73	370.73	370.73	370.73	370.73
322.46	322.46	322.46	322.46	322.46	322.46
279.41	279.41	279.41	279.41	279.41	279.41
241.15	241.15	241.15	241.15	241.15	241.15
207.25	207.25	207.25	207.25	207.25	207.25
177.38	177.38	177.38	177.38	177.38	177.38
151.47	151.47	151.47	151.47	151.47	151.47
129.29	129.29	129.29	129.29	129.29	129.29
110.36	110.36	110.36	110.36	110.36	110.36
94.19	94.19	94.19	94.19	94.19	94.19
80.41	80.41	80.41	80.41	80.41	80.41
68.67	68.67	68.67	68.67	68.67	68.67
58.69	58.69	58.69	58.69	58.69	58.69
50.20	50.20	50.20	50.20	50.20	50.20
42.98	42.98	42.98	42.98	42.98	42.98
36.83	36.83	36.83	36.83	36.83	36.83
31.58	31.58	31.58	31.58	31.58	31.58
27.11	27.11	27.11	27.11	27.11	27.11
12.86	12.86	12.86	12.86	12.86	12.86
6.31	6.31	6.31	6.31	6.31	6.31
3.20	3.20	3.20	3.20	3.20	3.20
1.67	1.67	1.67	1.67	1.67	1.67
0.89	0.89	0.89	0.89	0.89	0.89
0.06	0.06	0.06	0.06	0.06	0.06
0.00	0.00	0.00	0.00	0.00	0.00

Temperature (k)

number	clear sky	stratospheric	CO2 300ppm -600ppm	aerosol 0-1km	aerosol 0-2 km	aerosol 0-3km
1	294.00	294.00	294.00	294.00	294.00	294.00
2	294.00	294.00	294.00	294.00	294.00	294.00
3	294.00	294.00	294.00	294.00	294.00	294.00
4	294.00	294.00	294.00	294.00	294.00	294.00
5	293.99	293.99	293.99	293.99	293.99	293.99
6	293.96	293.96	293.96	293.96	293.96	293.96
7	293.87	293.87	293.87	293.87	293.87	293.87
8	293.60	293.60	293.60	293.60	293.60	293.60
9	292.72	292.72	292.72	292.72	292.72	292.72
10	290.00	290.00	290.00	290.00	290.00	290.00
11	285.00	285.00	285.00	285.00	285.00	285.00
12	279.00	279.00	279.00	279.00	279.00	279.00
13	273.00	273.00	273.00	273.00	273.00	273.00
14	267.10	267.10	267.10	267.10	267.10	267.10
15	261.00	261.00	261.00	261.00	261.00	261.00
16	254.70	254.70	254.70	254.70	254.70	254.70
17	248.20	248.20	248.20	248.20	248.20	248.20
18	241.70	241.70	241.70	241.70	241.70	241.70
19	235.20	235.20	235.20	235.20	235.20	235.20
20	228.80	228.80	228.80	228.80	228.80	228.80
21	222.30	222.30	222.30	222.30	222.30	222.30
22	216.90	216.90	216.90	216.90	216.90	216.90
23	215.80	215.80	215.80	215.80	215.80	215.80
24	215.80	215.80	215.80	215.80	215.80	215.80
25	215.80	215.80	215.80	215.80	215.80	215.80
26	215.80	215.80	215.80	215.80	215.80	215.80
27	216.00	216.00	216.00	216.00	216.00	216.00
28	217.00	217.00	217.00	217.00	217.00	217.00
29	218.20	218.20	218.20	218.20	218.20	218.20
30	219.40	219.40	219.40	219.40	219.40	219.40
31	220.60	220.60	220.60	220.60	220.60	220.60
32	221.80	221.80	221.80	221.80	221.80	221.80
33	223.00	223.00	223.00	223.00	223.00	223.00
34	224.20	224.20	224.20	224.20	224.20	224.20
35	234.20	234.20	234.20	234.20	234.20	234.20
36	245.30	245.30	245.30	245.30	245.30	245.30
37	257.50	257.50	257.50	257.50	257.50	257.50
38	269.70	269.70	269.70	269.70	269.70	269.70
39	276.20	276.20	276.20	276.20	276.20	276.20
40	219.10	219.10	219.10	219.10	219.10	219.10
41	209.90	209.90	209.90	209.90	209.90	209.90

Water Vapor (g/kg)

number	clear sky	stratospheric	CO2 300ppm -600ppm	aerosol 0-1km	aerosol 0-2 km	aerosol 0-3km
1	11.66	11.66	11.66	11.66	11.66	11.66
2	11.66	11.66	11.66	11.66	11.66	11.66
3	11.66	11.66	11.66	11.66	11.66	11.66
4	11.66	11.66	11.66	11.66	11.66	11.66
5	11.65	11.65	11.65	11.65	11.65	11.65
6	11.63	11.63	11.63	11.63	11.63	11.63
7	11.57	11.57	11.57	11.57	11.57	11.57
8	11.39	11.39	11.39	11.39	11.39	11.39
9	10.76	10.76	10.76	10.76	10.76	10.76
10	8.59	8.59	8.59	8.59	8.59	8.59
11	5.98	5.98	5.98	5.98	5.98	5.98
12	3.87	3.87	3.87	3.87	3.87	3.87
13	2.36	2.36	2.36	2.36	2.36	2.36
14	1.39	1.39	1.39	1.39	1.39	1.39
15	0.94	0.94	0.94	0.94	0.94	0.94
16	0.64	0.64	0.64	0.64	0.64	0.64
17	0.40	0.40	0.40	0.40	0.40	0.40
18	0.25	0.25	0.25	0.25	0.25	0.25
19	0.16	0.16	0.16	0.16	0.16	0.16
20	0.06	0.06	0.06	0.06	0.06	0.06
21	0.02	0.02	0.02	0.02	0.02	0.02
22	0.01	0.01	0.01	0.01	0.01	0.01
23	0.00	0.00	0.00	0.00	0.00	0.00
24	0.00	0.00	0.00	0.00	0.00	0.00
25	0.00	0.00	0.00	0.00	0.00	0.00
26	0.00	0.00	0.00	0.00	0.00	0.00
27	0.00	0.00	0.00	0.00	0.00	0.00
28	0.00	0.00	0.00	0.00	0.00	0.00
29	0.00	0.00	0.00	0.00	0.00	0.00
30	0.00	0.00	0.00	0.00	0.00	0.00
31	0.00	0.00	0.00	0.00	0.00	0.00
32	0.00	0.00	0.00	0.00	0.00	0.00
33	0.00	0.00	0.00	0.00	0.00	0.00
34	0.00	0.00	0.00	0.00	0.00	0.00
35	0.00	0.00	0.00	0.00	0.00	0.00
36	0.00	0.00	0.00	0.00	0.00	0.00
37	0.00	0.00	0.00	0.00	0.00	0.00
38	0.00	0.00	0.00	0.00	0.00	0.00
39	0.00	0.00	0.00	0.00	0.00	0.00
40	0.00	0.00	0.00	0.00	0.00	0.00
41	0.00	0.00	0.00	0.00	0.00	0.00

Middle heating rate altitude(Z(m))Lwhr

number	clear sky	stratospheric	CO2 300ppm -600ppm	aerosol 0-1km	aerosol 0-2 km	aerosol 0-3km
1	0.05	0.05	0.05	0.05	0.05	0.05
2	0.21	0.21	0.21	0.21	0.21	0.21
3	0.66	0.66	0.66	0.66	0.66	0.66
4	2.10	2.10	2.10	2.10	2.10	2.10
5	6.60	6.60	6.60	6.60	6.60	6.60
6	21.00	21.00	21.00	21.00	21.00	21.00
7	66.00	66.00	66.00	66.00	66.00	66.00
8	210.00	210.00	210.00	210.00	210.00	210.00
9	660.00	660.00	660.00	660.00	660.00	660.00
10	1500.00	1500.00	1500.00	1500.00	1500.00	1500.00
11	2500.00	2500.00	2500.00	2500.00	2500.00	2500.00
12	3500.00	3500.00	3500.00	3500.00	3500.00	3500.00
13	4500.00	4500.00	4500.00	4500.00	4500.00	4500.00
14	5500.00	5500.00	5500.00	5500.00	5500.00	5500.00
15	6500.00	6500.00	6500.00	6500.00	6500.00	6500.00
16	7500.00	7500.00	7500.00	7500.00	7500.00	7500.00
17	8500.00	8500.00	8500.00	8500.00	8500.00	8500.00
18	9500.00	9500.00	9500.00	9500.00	9500.00	9500.00
19	10500.00	10500.00	10500.00	10500.00	10500.00	10500.00
20	11500.00	11500.00	11500.00	11500.00	11500.00	11500.00
21	12500.00	12500.00	12500.00	12500.00	12500.00	12500.00
22	13500.00	13500.00	13500.00	13500.00	13500.00	13500.00
23	14500.00	14500.00	14500.00	14500.00	14500.00	14500.00
24	15500.00	15500.00	15500.00	15500.00	15500.00	15500.00
25	16500.00	16500.00	16500.00	16500.00	16500.00	16500.00
26	17500.00	17500.00	17500.00	17500.00	17500.00	17500.00
27	18500.00	18500.00	18500.00	18500.00	18500.00	18500.00
28	19500.00	19500.00	19500.00	19500.00	19500.00	19500.00
29	20500.00	20500.00	20500.00	20500.00	20500.00	20500.00
30	21500.00	21500.00	21500.00	21500.00	21500.00	21500.00
31	22500.00	22500.00	22500.00	22500.00	22500.00	22500.00
32	23500.00	23500.00	23500.00	23500.00	23500.00	23500.00
33	24500.00	24500.00	24500.00	24500.00	24500.00	24500.00
34	27500.00	27500.00	27500.00	27500.00	27500.00	27500.00
35	32500.00	32500.00	32500.00	32500.00	32500.00	32500.00
36	37500.00	37500.00	37500.00	37500.00	37500.00	37500.00
37	42500.00	42500.00	42500.00	42500.00	42500.00	42500.00
38	47500.00	47500.00	47500.00	47500.00	47500.00	47500.00
39	60000.00	60000.00	60000.00	60000.00	60000.00	60000.00
40	87000.00	87000.00	87000.00	87000.00	87000.00	87000.00
41	152000.00	52000.00	52000.00	52000.00	152000.00	52000.00

Cloud water path g/m2 liquid/ice

mber	clear sky	stratospheric	CO2 300ppm -600ppm	aerosol 0-1km	aerosol 0-2 km	aerosol 0-3km
1	0.00	0.00	0.00	0.00	0.00	0.00
2	0.00	0.00	0.00	0.00	0.00	0.00
3	0.00	0.00	0.00	0.00	0.00	0.00
4	0.00	0.00	0.00	0.00	0.00	0.00
5	0.00	0.00	0.00	0.00	0.00	0.00
6	0.00	0.00	0.00	0.00	0.00	0.00
7	0.00	0.00	0.00	0.00	0.00	0.00
8	0.00	0.00	0.00	0.00	0.00	0.00
9	0.00	0.00	0.00	0.00	0.00	0.00
10	0.00	0.00	0.00	0.00	0.00	0.00
11	0.00	0.00	0.00	0.00	0.00	0.00
12	0.00	0.00	0.00	0.00	0.00	0.00
13	0.00	0.00	0.00	0.00	0.00	0.00
14	0.00	0.00	0.00	0.00	0.00	0.00
15	0.00	0.00	0.00	0.00	0.00	0.00
16	0.00	0.00	0.00	0.00	0.00	0.00
17	0.00	0.00	0.00	0.00	0.00	0.00
18	0.00	0.00	0.00	0.00	0.00	0.00
19	0.00	0.00	0.00	0.00	0.00	0.00
20	0.00	0.00	0.00	0.00	0.00	0.00
21	0.00	0.00	0.00	0.00	0.00	0.00
22	0.00	0.00	0.00	0.00	0.00	0.00
23	0.00	0.00	0.00	0.00	0.00	0.00
24	0.00	0.00	0.00	0.00	0.00	0.00
25	0.00	0.00	0.00	0.00	0.00	0.00
26	0.00	0.00	0.00	0.00	0.00	0.00
27	0.00	0.00	0.00	0.00	0.00	0.00
28	0.00	0.00	0.00	0.00	0.00	0.00
29	0.00	0.00	0.00	0.00	0.00	0.00
30	0.00	0.00	0.00	0.00	0.00	0.00
31	0.00	0.00	0.00	0.00	0.00	0.00
32	0.00	0.00	0.00	0.00	0.00	0.00
33	0.00	0.00	0.00	0.00	0.00	0.00
34	0.00	0.00	0.00	0.00	0.00	0.00
35	0.00	0.00	0.00	0.00	0.00	0.00
36	0.00	0.00	0.00	0.00	0.00	0.00
37	0.00	0.00	0.00	0.00	0.00	0.00
38	0.00	0.00	0.00	0.00	0.00	0.00
39	0.00	0.00	0.00	0.00	0.00	0.00
40	0.00	0.00	0.00	0.00	0.00	0.00
41	0.00	0.00	0.00	0.00	0.00	0.00

Aerosol visible extinction coefficient

number	clear sky	stratospheric	CO2 300ppm -600ppm	aerosol 0-1km	aerosol 0-2 km	aerosol 0-3kn
1	0.00	0.00	0.00	0.10	0.10	0.10
2	0.00	0.00	0.00	0.10	0.10	0.10
3	0.00	0.00	0.00	0.10	0.10	0.10
4	0.00	0.00	0.00	0.10	0.10	0.10
5	0.00	0.00	0.00	0.10	0.10	0.10
6	0.00	0.00	0.00	0.10	0.10	0.10
7	0.00	0.00	0.00	0.10	0.10	0.10
8	0.00	0.00	0.00	0.10	0.10	0.10
9	0.00	0.00	0.00	0.10	0.10	0.10
10	0.00	0.00	0.00	0.10	0.10	0.10
11	0.00	0.00	0.00	0.00	0.10	0.10
12	0.00	0.00	0.00	0.00	0.00	0.00
13	0.00	0.00	0.00	0.00	0.00	0.00
14	0.00	0.00	0.00	0.00	0.00	0.00
15	0.00	0.00	0.00	0.00	0.00	0.00
16	0.00	0.00	0.00	0.00	0.00	0.00
17	0.00	0.00	0.00	0.00	0.00	0.00
18	0.00	0.00	0.00	0.00	0.00	0.00
19	0.00	0.00	0.00	0.00	0.00	0.00
20	0.00	0.00	0.00	0.00	0.00	0.00
21	0.00	0.00	0.00	0.00	0.00	0.00
22	0.00	0.00	0.00	0.00	0.00	0.00
23	0.00	0.10	0.00	0.00	0.00	0.00
24	0.00	0.10	0.00	0.00	0.00	0.00
25	0.00	0.10	0.00	0.00	0.00	0.00
26	0.00	0.10	0.00	0.00	0.00	0.00
27	0.00	0.10	0.00	0.00	0.00	0.00
28	0.00	0.10	0.00	0.00	0.00	0.00
29	0.00	0.10	0.00	0.00	0.00	0.00
30	0.00	0.10	0.00	0.00	0.00	0.00
31	0.00	0.10	0.00	0.00	0.00	0.00
32	0.00	0.10	0.00	0.00	0.00	0.00
33	0.00	0.00	0.00	0.00	0.00	0.00
34	0.00	0.00	0.00	0.00	0.00	0.00
35	0.00	0.00	0.00	0.00	0.00	0.00
36	0.00	0.00	0.00	0.00	0.00	0.00
37	0.00	0.00	0.00	0.00	0.00	0.00
38	0.00	0.00	0.00	0.00	0.00	0.00
39	0.00	0.00	0.00	0.00	0.00	0.00
40	0.00	0.00	0.00	0.00	0.00	0.00
41	0.00	0.00	0.00	0.00	0.00	0.00

Appendix B

LW Radiation scheme output for the clear sky, stratospheric aerosol, doubled CO_2 and constant β_{ae} cases

Clear sky reference case

```
38: Command not found.
kruuna.helsinki.fi% 39 50000.00     0.89   276.20     0.00     0.54   287.81   287.27    -3.05 60000.00
 0.00
39: Command not found.
kruuna.helsinki.fi% a.out
  0   294.00   294.00     1.00     2.96   300.00     0.76     1.00     0.00     0.00
  1
  1     0.00  1013.00   294.00    11.66   344.76   423.62    78.85    -3.78     0.05     0.00     0.00
  2     0.10  1012.99   294.00    11.66   344.76   423.62    78.86    -3.75     0.21     0.00     0.00
  3     0.32  1012.96   294.00    11.66   344.75   423.62    78.87    -3.73     0.66     0.00     0.00
  4     1.00  1012.88   294.00    11.66   344.71   423.62    78.91    -3.72     2.10     0.00     0.00
  5     3.20  1012.62   293.99    11.65   344.59   423.61    79.02    -3.73     6.60     0.00     0.00
  6    10.00  1011.82   293.96    11.63   344.20   423.58    79.37    -3.73    21.00     0.00     0.00
  7    32.00  1009.24   293.87    11.57   342.93   423.45    80.52    -3.79    66.00     0.00     0.00
  8   100.00  1001.29   293.60    11.39   338.85   422.93    84.08    -3.75   210.00     0.00     0.00
  9   320.00   975.94   292.72    10.76   325.62   420.96    95.33    -3.07   660.00     0.00     0.00
 10  1000.00   901.13   290.00     8.59   291.36   413.91   122.55    -2.39  1500.00     0.00     0.00
 11  2000.00   800.15   285.00     5.98   248.64   399.76   151.12    -1.79  2500.00     0.00     0.00
 12  3000.00   708.84   279.00     3.87   211.81   382.35   170.54    -1.52  3500.00     0.00     0.00
 13  4000.00   626.30   273.00     2.36   180.39   365.80   185.42    -1.49  4500.00     0.00     0.00
 14  5000.00   551.86   267.10     1.39   153.10   351.63   198.54    -1.49  5500.00     0.00     0.00
 15  6000.00   484.88   261.00     0.94   128.97   339.35   210.39    -1.58  6500.00     0.00     0.00
 16  7000.00   424.70   254.70     0.64   106.80   328.42   221.62    -1.68  7500.00     0.00     0.00
 17  8000.00   370.73   248.20     0.40    86.53   318.88   232.35    -1.79  8500.00     0.00     0.00
 18  9000.00   322.46   241.70     0.25    68.27   310.85   242.58    -2.04  9500.00     0.00     0.00
 19 10000.00   279.41   235.20     0.16    51.28   304.26   252.98    -2.16 10500.00     0.00     0.00
 20 11000.00   241.15   228.80     0.06    36.36   299.15   262.79    -1.45 11500.00     0.00     0.00
 21 12000.00   207.25   222.30     0.02    26.76   295.37   268.61    -0.48 12500.00     0.00     0.00
 22 13000.00   177.38   216.90     0.01    22.38   292.67   270.29    -0.06 13500.00     0.00     0.00
 23 14000.00   151.47   215.80     0.00    20.52   290.99   270.47    -0.16 14500.00     0.00     0.00
 24 15000.00   129.29   215.80     0.00    19.06   289.95   270.88    -0.26 15500.00     0.00     0.00
 25 16000.00   110.36   215.80     0.00    17.72   289.18   271.46    -0.29 16500.00     0.00     0.00
 26 17000.00    94.19   215.80     0.00    16.49   288.50   272.01    -0.28 17500.00     0.00     0.00
 27 18000.00    80.41   216.00     0.00    15.41   287.89   272.48    -0.32 18500.00     0.00     0.00
 28 19000.00    68.67   217.00     0.00    14.44   287.36   272.92    -0.43 19500.00     0.00     0.00
 29 20000.00    58.69   218.20     0.00    13.52   286.95   273.43    -0.56 20500.00     0.00     0.00
 30 21000.00    50.20   219.40     0.00    12.63   286.62   274.00    -0.69 21500.00     0.00     0.00
 31 22000.00    42.98   220.60     0.00    11.77   286.36   274.59    -0.84 22500.00     0.00     0.00
 32 23000.00    36.83   221.80     0.00    10.96   286.16   275.20    -0.96 23500.00     0.00     0.00
 33 24000.00    31.58   223.00     0.00    10.23   286.03   275.80    -0.75 24500.00     0.00     0.00
 34 25000.00    27.11   224.20     0.00     9.75   285.95   276.19    -1.88 27500.00     0.00     0.00
 35 30000.00    12.86   234.20     0.00     6.62   285.99   279.37    -3.82 32500.00     0.00     0.00
 36 35000.00     6.31   245.30     0.00     4.24   286.58   282.34    -5.99 37500.00     0.00     0.00
 37 40000.00     3.20   257.50     0.00     2.61   287.16   284.54    -8.85 42500.00     0.00     0.00
 38 45000.00     1.67   269.70     0.00     1.44   287.58   286.14   -12.25 47500.00     0.00     0.00
 39 50000.00     0.89   276.20     0.00     0.54   287.81   287.27    -3.05 60000.00     0.00     0.00
 40 70000.00     0.06   219.10     0.00     0.02   287.59   287.57    -0.06 87000.00     0.00     0.00
 41104000.00     0.00   209.90     0.00     0.00   287.57   287.57    -1.86152000.00     0.00     0.00
 Note: IEEE floating-point exception flags raised:
    Inexact;  Underflow;
 See the Numerical Computation Guide, ieee_flags(3M)
kruuna.helsinki.fi%
```

Stratospheric aerosol case (constant β_{ae} of 0.1 km^{-1} at 0.55 μm)

```
NOTICE: Invoking /opt/SUNWspro/bin/f90 -f77 -ftrap=%none enbm.f
enbm.f:
 MAIN enbm:
        b:
kruuna.helsinki.fi% a.out
  0   294.00   294.00     1.00     2.96   300.00     0.76     1.00     0.00     1.00
  1
  1     0.00  1013.00   294.00    11.66   346.47   423.62    77.14    -3.61     0.05     0.00     0.00
  2     0.10  1012.99   294.00    11.66   346.47   423.62    77.15    -3.73     0.21     0.00     0.00
  3     0.32  1012.96   294.00    11.66   346.46   423.62    77.16    -3.67     0.66     0.00     0.00
  4     1.00  1012.88   294.00    11.66   346.42   423.62    77.20    -3.66     2.10     0.00     0.00
  5     3.20  1012.62   293.99    11.65   346.30   423.61    77.31    -3.67     6.60     0.00     0.00
  6    10.00  1011.82   293.96    11.63   345.92   423.58    77.66    -3.67    21.00     0.00     0.00
  7    32.00  1009.24   293.87    11.57   344.67   423.45    78.78    -3.73    66.00     0.00     0.00
  8   100.00  1001.29   293.60    11.39   340.64   422.93    82.29    -3.68   210.00     0.00     0.00
  9   320.00   975.94   292.72    10.76   327.61   420.96    93.34    -3.00   660.00     0.00     0.00
 10  1000.00   901.13   290.00     8.59   293.94   413.91   119.97    -2.32  1500.00     0.00     0.00
 11  2000.00   800.15   285.00     5.98   252.00   399.76   147.76    -1.73  2500.00     0.00     0.00
 12  3000.00   708.84   279.00     3.87   215.87   382.35   166.47    -1.46  3500.00     0.00     0.00
 13  4000.00   626.30   273.00     2.36   185.09   365.80   180.71    -1.42  4500.00     0.00     0.00
 14  5000.00   551.86   267.10     1.39   158.41   351.63   193.22    -1.42  5500.00     0.00     0.00
 15  6000.00   484.88   261.00     0.94   134.85   339.35   204.50    -1.49  6500.00     0.00     0.00
 16  7000.00   424.70   254.70     0.64   113.27   328.42   215.15    -1.58  7500.00     0.00     0.00
 17  8000.00   370.73   248.20     0.40    93.61   318.88   225.27    -1.68  8500.00     0.00     0.00
 18  9000.00   322.46   241.70     0.25    75.96   310.85   234.89    -1.92  9500.00     0.00     0.00
 19 10000.00   279.41   235.20     0.16    59.60   304.26   244.66    -2.04 10500.00     0.00     0.00
 20 11000.00   241.15   228.80     0.06    45.26   299.15   253.89    -1.35 11500.00     0.00     0.00
 21 12000.00   207.25   222.30     0.02    36.04   295.37   259.32    -0.42 12500.00     0.00     0.00
 22 13000.00   177.38   216.90     0.01    31.87   292.67   260.80     0.23 13500.00     0.00     0.00
 23 14000.00   151.47   215.80     0.00    29.70   289.79   260.10     0.45 14500.00     0.00     0.10
 24 15000.00   129.29   215.80     0.00    27.47   286.39   258.93     0.41 15500.00     0.00     0.10
 25 16000.00   110.36   215.80     0.00    25.32   283.33   258.01     0.44 16500.00     0.00     0.10
 26 17000.00    94.19   215.80     0.00    23.25   280.42   257.17     0.51 17500.00     0.00     0.10
 27 18000.00    80.41   216.00     0.00    21.29   277.62   256.33     0.53 18500.00     0.00     0.10
 28 19000.00    68.67   217.00     0.00    19.40   274.99   255.59     0.45 19500.00     0.00     0.10
 29 20000.00    58.69   218.20     0.00    17.49   272.55   255.05     0.33 20500.00     0.00     0.10
 30 21000.00    50.20   219.40     0.00    15.55   270.27   254.72     0.20 21500.00     0.00     0.10
 31 22000.00    42.98   220.60     0.00    13.58   268.12   254.55     0.03 22500.00     0.00     0.10
 32 23000.00    36.83   221.80     0.00    11.59   266.11   254.53    -0.59 23500.00     0.00     0.10
 33 24000.00    31.58   223.00     0.00    10.23   265.12   254.89    -0.83 24500.00     0.00     0.00
 34 25000.00    27.11   224.20     0.00     9.75   265.08   255.33    -1.97 27500.00     0.00     0.00
 35 30000.00    12.86   234.20     0.00     6.62   265.27   258.66    -3.91 32500.00     0.00     0.00
 36 35000.00     6.31   245.30     0.00     4.24   265.94   261.70    -6.07 37500.00     0.00     0.00
 37 40000.00     3.20   257.50     0.00     2.61   266.55   263.94    -8.93 42500.00     0.00     0.00
 38 45000.00     1.67   269.70     0.00     1.44   266.99   265.55   -12.31 47500.00     0.00     0.00
 39 50000.00     0.89   276.20     0.00     0.54   267.22   266.68    -3.11 60000.00     0.00     0.00
 40 70000.00     0.06   219.10     0.00     0.02   267.01   266.99    -0.09 87000.00     0.00     0.00
 41104000.00     0.00   209.90     0.00     0.00   266.99   266.99    -1.86152000.00     0.00     0.00
 Note: IEEE floating-point exception flags raised:
    Inexact;  Underflow;
 See the Numerical Computation Guide, ieee_flags(3M)
kruuna.helsinki.fi%
```

Doubled CO_2 case (600 ppm)

```
NOTICE: Invoking /opt/SUNWspro/bin/f90 -f77 -ftrap=%none enbm.f
enbm.f:
 MAIN enbm:
        b:
kruuna.helsinki.fi% a.out
  0   294.00   294.00     1.00     2.96   600.00     0.76     1.00     0.00     0.00
  1
  1     0.00  1013.00   294.00    11.66   346.66   423.62    76.96    -3.63     0.05     0.00     0.00
  2     0.10  1012.99   294.00    11.66   346.66   423.62    76.96    -3.69     0.21     0.00     0.00
  3     0.32  1012.96   294.00    11.66   346.65   423.62    76.97    -3.67     0.66     0.00     0.00
  4     1.00  1012.88   294.00    11.66   346.61   423.62    77.01    -3.65     2.10     0.00     0.00
  5     3.20  1012.62   293.99    11.65   346.49   423.61    77.12    -3.67     6.60     0.00     0.00
  6    10.00  1011.82   293.96    11.63   346.11   423.58    77.47    -3.67    21.00     0.00     0.00
  7    32.00  1009.24   293.87    11.57   344.85   423.44    78.59    -3.73    66.00     0.00     0.00
  8   100.00  1001.29   293.60    11.39   340.81   422.91    82.10    -3.69   210.00     0.00     0.00
  9   320.00   975.94   292.72    10.76   327.74   420.91    93.17    -3.00   660.00     0.00     0.00
 10  1000.00   901.13   290.00     8.59   294.05   413.81   119.76    -2.32  1500.00     0.00     0.00
 11  2000.00   800.15   285.00     5.98   251.97   399.51   147.54    -1.74  2500.00     0.00     0.00
 12  3000.00   708.84   279.00     3.87   215.45   381.82   166.36    -1.48  3500.00     0.00     0.00
 13  4000.00   626.30   273.00     2.36   184.09   364.93   180.84    -1.46  4500.00     0.00     0.00
 14  5000.00   551.86   267.10     1.39   156.67   350.41   193.74    -1.48  5500.00     0.00     0.00
 15  6000.00   484.88   261.00     0.94   132.31   337.76   205.46    -1.56  6500.00     0.00     0.00
 16  7000.00   424.70   254.70     0.64   109.93   326.47   216.54    -1.66  7500.00     0.00     0.00
 17  8000.00   370.73   248.20     0.40    89.40   316.59   227.18    -1.78  8500.00     0.00     0.00
 18  9000.00   322.46   241.70     0.25    70.89   308.25   237.36    -2.04  9500.00     0.00     0.00
 19 10000.00   279.41   235.20     0.16    53.64   301.38   247.74    -2.17 10500.00     0.00     0.00
 20 11000.00   241.15   228.80     0.06    38.46   296.04   257.59    -1.46 11500.00     0.00     0.00
 21 12000.00   207.25   222.30     0.02    26.61   292.07   263.47    -0.46 12500.00     0.00     0.00
 22 13000.00   177.38   216.90     0.01    24.15   289.24   265.09    -0.04 13500.00     0.00     0.00
 23 14000.00   151.47   215.80     0.00    22.31   287.53   265.22    -0.16 14500.00     0.00     0.00
 24 15000.00   129.29   215.80     0.00    20.89   286.53   265.64    -0.28 15500.00     0.00     0.00
 25 16000.00   110.36   215.80     0.00    19.55   285.81   266.26    -0.31 16500.00     0.00     0.00
 26 17000.00    94.19   215.80     0.00    18.33   285.18   266.86    -0.30 17500.00     0.00     0.00
 27 18000.00    80.41   216.00     0.00    17.26   284.60   267.35    -0.34 18500.00     0.00     0.00
 28 19000.00    68.67   217.00     0.00    16.31   284.12   267.82    -0.46 19500.00     0.00     0.00
 29 20000.00    58.69   218.20     0.00    15.39   283.76   268.37    -0.61 20500.00     0.00     0.00
 30 21000.00    50.20   219.40     0.00    14.50   283.49   268.98    -0.75 21500.00     0.00     0.00
 31 22000.00    42.98   220.60     0.00    13.64   283.27   269.63    -0.92 22500.00     0.00     0.00
 32 23000.00    36.83   221.80     0.00    12.82   283.12   270.30    -1.06 23500.00     0.00     0.00
 33 24000.00    31.58   223.00     0.00    12.08   283.03   270.95    -0.72 24500.00     0.00     0.00
 34 25000.00    27.11   224.20     0.00    11.65   282.98   271.33    -2.18 27500.00     0.00     0.00
 35 30000.00    12.86   234.20     0.00     8.21   283.22   275.02    -4.68 32500.00     0.00     0.00
 36 35000.00     6.31   245.30     0.00     5.40   284.05   278.65    -7.53 37500.00     0.00     0.00
 37 40000.00     3.20   257.50     0.00     3.38   284.80   281.42   -11.33 42500.00     0.00     0.00
 38 45000.00     1.67   269.70     0.00     1.89   285.36   283.47   -16.14 47500.00     0.00     0.00
 39 50000.00     0.89   276.20     0.00     0.71   285.66   284.96    -4.01 60000.00     0.00     0.00
 40 70000.00     0.06   219.10     0.00     0.02   285.37   285.35    -0.08 87000.00     0.00     0.00
 41104000.00     0.00   209.90     0.00     0.00   285.35   285.35    -2.53152000.00     0.00     0.00
 Note: IEEE floating-point exception flags raised:
    Inexact;  Underflow;
 See the Numerical Computation Guide, ieee_flags(3M)
kruuna.helsinki.fi%
```

Aerosol with constant β_{ae} of 0.1 km^{-1} at 0.55 µm between 0 - 1 km

```
NOTICE: Invoking /opt/SUNWspro/bin/f90 -f77 -ftrap=%none enbm.f
enbm.f:
 MAIN enbm:
       b:
kruuna.helsinki.fi% a.out
  0   294.00   294.00     1.00     2.96   300.00     0.76     1.00     0.00     0.15
  1
  1     0.00  1013.00   294.00    11.66   346.41   423.62    77.21    -3.87     0.05     0.00     0.10
  2     0.10  1012.99   294.00    11.66   346.40   423.62    77.21    -3.78     0.21     0.00     0.10
  3     0.32  1012.96   294.00    11.66   346.39   423.62    77.22    -3.75     0.66     0.00     0.10
  4     1.00  1012.88   294.00    11.66   346.36   423.62    77.26    -3.75     2.10     0.00     0.10
  5     3.20  1012.62   293.99    11.65   346.23   423.61    77.38    -3.76     6.60     0.00     0.10
  6    10.00  1011.82   293.96    11.63   345.85   423.58    77.73    -3.76    21.00     0.00     0.10
  7    32.00  1009.24   293.87    11.57   344.56   423.45    78.88    -3.82    66.00     0.00     0.10
  8   100.00  1001.29   293.60    11.39   340.45   422.93    82.49    -3.79   210.00     0.00     0.10
  9   320.00   975.94   292.72    10.76   327.08   420.95    93.87    -3.15   660.00     0.00     0.10
 10  1000.00   901.13   290.00     8.59   292.10   413.85   121.75    -2.44  1500.00     0.00     0.10
 11  2000.00   800.15   285.00     5.98   248.64   399.62   150.98    -1.80  2500.00     0.00     0.00
 12  3000.00   708.84   279.00     3.87   211.81   382.22   170.41    -1.52  3500.00     0.00     0.00
 13  4000.00   626.30   273.00     2.36   180.39   365.68   185.29    -1.49  4500.00     0.00     0.00
 14  5000.00   551.86   267.10     1.39   153.10   351.51   198.42    -1.49  5500.00     0.00     0.00
 15  6000.00   484.88   261.00     0.94   128.97   339.23   210.27    -1.58  6500.00     0.00     0.00
 16  7000.00   424.70   254.70     0.64   106.80   328.30   221.50    -1.68  7500.00     0.00     0.00
 17  8000.00   370.73   248.20     0.40    86.53   318.76   232.23    -1.79  8500.00     0.00     0.00
 18  9000.00   322.46   241.70     0.25    68.27   310.73   242.46    -2.04  9500.00     0.00     0.00
 19 10000.00   279.41   235.20     0.16    51.28   304.14   252.86    -2.16 10500.00     0.00     0.00
 20 11000.00   241.15   228.80     0.06    36.36   299.03   262.67    -1.45 11500.00     0.00     0.00
 21 12000.00   207.25   222.30     0.02    26.76   295.25   268.49    -0.48 12500.00     0.00     0.00
 22 13000.00   177.38   216.90     0.01    22.38   292.55   270.17    -0.06 13500.00     0.00     0.00
 23 14000.00   151.47   215.80     0.00    20.52   290.87   270.36    -0.16 14500.00     0.00     0.00
 24 15000.00   129.29   215.80     0.00    19.06   289.83   270.77    -0.26 15500.00     0.00     0.00
 25 16000.00   110.36   215.80     0.00    17.72   289.06   271.34    -0.29 16500.00     0.00     0.00
 26 17000.00    94.19   215.80     0.00    16.49   288.39   271.90    -0.28 17500.00     0.00     0.00
 27 18000.00    80.41   216.00     0.00    15.41   287.77   272.36    -0.32 18500.00     0.00     0.00
 28 19000.00    68.67   217.00     0.00    14.44   287.25   272.81    -0.43 19500.00     0.00     0.00
 29 20000.00    58.69   218.20     0.00    13.52   286.84   273.32    -0.57 20500.00     0.00     0.00
 30 21000.00    50.20   219.40     0.00    12.63   286.51   273.89    -0.69 21500.00     0.00     0.00
 31 22000.00    42.98   220.60     0.00    11.77   286.25   274.48    -0.84 22500.00     0.00     0.00
 32 23000.00    36.83   221.80     0.00    10.96   286.05   275.09    -0.96 23500.00     0.00     0.00
 33 24000.00    31.58   223.00     0.00    10.23   285.92   275.69    -0.75 24500.00     0.00     0.00
 34 25000.00    27.11   224.20     0.00     9.75   285.83   276.08    -1.88 27500.00     0.00     0.00
 35 30000.00    12.86   234.20     0.00     6.62   285.88   279.26    -3.82 32500.00     0.00     0.00
 36 35000.00     6.31   245.30     0.00     4.24   286.47   282.23    -5.99 37500.00     0.00     0.00
 37 40000.00     3.20   257.50     0.00     2.61   287.05   284.44    -8.85 42500.00     0.00     0.00
 38 45000.00     1.67   269.70     0.00     1.44   287.48   286.03   -12.25 47500.00     0.00     0.00
 39 50000.00     0.89   276.20     0.00     0.54   287.70   287.16    -3.06 60000.00     0.00     0.00
 40 70000.00     0.06   219.10     0.00     0.02   287.48   287.47    -0.06 87000.00     0.00     0.00
 41104000.00     0.00   209.90     0.00     0.00   287.47   287.47    -1.86152000.00     0.00     0.00
 Note: IEEE floating-point exception flags raised:
    Inexact;  Underflow;
 See the Numerical Computation Guide, ieee_flags(3M)
kruuna.helsinki.fi%
```

Aerosol with constant β_{ae} of 0.1 km^{-1} at 0.55 µm between 0 - 2 km

```
kruuna.helsinki.fi% f77 enbm.f
NOTICE: Invoking /opt/SUNWspro/bin/f90 -f77 -ftrap=%none enbm.f
enbm.f:
 MAIN enbm:
        b:
kruuna.helsinki.fi% a.out
  0   294.00   294.00     1.00     2.96   300.00     0.76     1.00     0.00     0.25
  1
  1     0.00  1013.00   294.00    11.66   347.35   423.62    76.27    -3.72     0.05     0.00     0.10
  2     0.10  1012.99   294.00    11.66   347.34   423.62    76.28    -3.77     0.21     0.00     0.10
  3     0.32  1012.96   294.00    11.66   347.33   423.62    76.29    -3.73     0.66     0.00     0.10
  4     1.00  1012.88   294.00    11.66   347.29   423.62    76.32    -3.72     2.10     0.00     0.10
  5     3.20  1012.62   293.99    11.65   347.17   423.61    76.44    -3.73     6.60     0.00     0.10
  6    10.00  1011.82   293.96    11.63   346.79   423.58    76.79    -3.73    21.00     0.00     0.10
  7    32.00  1009.24   293.87    11.57   345.51   423.45    77.93    -3.79    66.00     0.00     0.10
  8   100.00  1001.29   293.60    11.39   341.43   422.93    81.50    -3.76   210.00     0.00     0.10
  9   320.00   975.94   292.72    10.76   328.16   420.95    92.79    -3.11   660.00     0.00     0.10
 10  1000.00   901.13   290.00     8.59   293.48   413.85   120.37    -2.48  1500.00     0.00     0.10
 11  2000.00   800.15   285.00     5.98   249.47   399.52   150.05    -1.86  2500.00     0.00     0.10
 12  3000.00   708.84   279.00     3.87   211.81   381.95   170.14    -1.52  3500.00     0.00     0.00
 13  4000.00   626.30   273.00     2.36   180.39   365.43   185.04    -1.49  4500.00     0.00     0.00
 14  5000.00   551.86   267.10     1.39   153.10   351.27   198.17    -1.49  5500.00     0.00     0.00
 15  6000.00   484.88   261.00     0.94   128.97   338.99   210.03    -1.58  6500.00     0.00     0.00
 16  7000.00   424.70   254.70     0.64   106.80   328.06   221.26    -1.68  7500.00     0.00     0.00
 17  8000.00   370.73   248.20     0.40    86.53   318.52   231.99    -1.79  8500.00     0.00     0.00
 18  9000.00   322.46   241.70     0.25    68.27   310.50   242.22    -2.04  9500.00     0.00     0.00
 19 10000.00   279.41   235.20     0.16    51.28   303.91   252.62    -2.16 10500.00     0.00     0.00
 20 11000.00   241.15   228.80     0.06    36.36   298.79   262.43    -1.45 11500.00     0.00     0.00
 21 12000.00   207.25   222.30     0.02    26.76   295.01   268.26    -0.48 12500.00     0.00     0.00
 22 13000.00   177.38   216.90     0.01    22.38   292.32   269.94    -0.06 13500.00     0.00     0.00
 23 14000.00   151.47   215.80     0.00    20.52   290.64   270.12    -0.16 14500.00     0.00     0.00
 24 15000.00   129.29   215.80     0.00    19.06   289.60   270.54    -0.26 15500.00     0.00     0.00
 25 16000.00   110.36   215.80     0.00    17.72   288.83   271.11    -0.29 16500.00     0.00     0.00
 26 17000.00    94.19   215.80     0.00    16.49   288.16   271.67    -0.29 17500.00     0.00     0.00
 27 18000.00    80.41   216.00     0.00    15.41   287.55   272.13    -0.32 18500.00     0.00     0.00
 28 19000.00    68.67   217.00     0.00    14.44   287.02   272.58    -0.43 19500.00     0.00     0.00
 29 20000.00    58.69   218.20     0.00    13.52   286.61   273.09    -0.57 20500.00     0.00     0.00
 30 21000.00    50.20   219.40     0.00    12.63   286.29   273.66    -0.69 21500.00     0.00     0.00
 31 22000.00    42.98   220.60     0.00    11.77   286.03   274.26    -0.84 22500.00     0.00     0.00
 32 23000.00    36.83   221.80     0.00    10.96   285.83   274.87    -0.96 23500.00     0.00     0.00
 33 24000.00    31.58   223.00     0.00    10.23   285.70   275.47    -0.75 24500.00     0.00     0.00
 34 25000.00    27.11   224.20     0.00     9.75   285.61   275.86    -1.89 27500.00     0.00     0.00
 35 30000.00    12.86   234.20     0.00     6.62   285.66   279.05    -3.82 32500.00     0.00     0.00
 36 35000.00     6.31   245.30     0.00     4.24   286.26   282.01    -5.99 37500.00     0.00     0.00
 37 40000.00     3.20   257.50     0.00     2.61   286.83   284.22    -8.85 42500.00     0.00     0.00
 38 45000.00     1.67   269.70     0.00     1.44   287.26   285.82   -12.25 47500.00     0.00     0.00
 39 50000.00     0.89   276.20     0.00     0.54   287.49   286.95    -3.06 60000.00     0.00     0.00
 40 70000.00     0.06   219.10     0.00     0.02   287.27   287.25    -0.06 87000.00     0.00     0.00
 41104000.00     0.00   209.90     0.00     0.00   287.25   287.25    -1.86152000.00     0.00     0.00
 Note: IEEE floating-point exception flags raised:
    Inexact;  Underflow;
 See the Numerical Computation Guide, ieee_flags(3M)
kruuna.helsinki.fi%
```

Aerosol with constant β_{ae} of 0.1 km^{-1} at 0.55 µm between 0 - 3 km

```
kruuna.helsinki.fi% f77 enbm.f
NOTICE: Invoking /opt/SUNWspro/bin/f90 -f77 -ftrap=%none enbm.f
enbm.f:
 MAIN enbm:
        b:
kruuna.helsinki.fi% a.out
  0   294.00   294.00     1.00     2.96   300.00     0.76     1.00     0.00     0.35
  1
  1     0.00  1013.00   294.00    11.66   348.17   423.62    75.45    -3.72     0.05     0.00     0.10
  2     0.10  1012.99   294.00    11.66   348.16   423.62    75.46    -3.74     0.21     0.00     0.10
  3     0.32  1012.96   294.00    11.66   348.15   423.62    75.47    -3.70     0.66     0.00     0.10
  4     1.00  1012.88   294.00    11.66   348.11   423.62    75.50    -3.69     2.10     0.00     0.10
  5     3.20  1012.62   293.99    11.65   347.99   423.61    75.62    -3.70     6.60     0.00     0.10
  6    10.00  1011.82   293.96    11.63   347.61   423.58    75.97    -3.70    21.00     0.00     0.10
  7    32.00  1009.24   293.87    11.57   346.34   423.45    77.10    -3.76    66.00     0.00     0.10
  8   100.00  1001.29   293.60    11.39   342.29   422.93    80.65    -3.73   210.00     0.00     0.10
  9   320.00   975.94   292.72    10.76   329.10   420.95    91.84    -3.08   660.00     0.00     0.10
 10  1000.00   901.13   290.00     8.59   294.69   413.85   119.16    -2.45  1500.00     0.00     0.10
 11  2000.00   800.15   285.00     5.98   251.02   399.52   148.50    -1.90  2500.00     0.00     0.10
 12  3000.00   708.84   279.00     3.87   212.68   381.77   169.09    -1.59  3500.00     0.00     0.10
 13  4000.00   626.30   273.00     2.36   180.39   364.98   184.59    -1.49  4500.00     0.00     0.00
 14  5000.00   551.86   267.10     1.39   153.10   350.84   197.74    -1.49  5500.00     0.00     0.00
 15  6000.00   484.88   261.00     0.94   128.97   338.57   209.60    -1.58  6500.00     0.00     0.00
 16  7000.00   424.70   254.70     0.64   106.80   327.64   220.84    -1.68  7500.00     0.00     0.00
 17  8000.00   370.73   248.20     0.40    86.53   318.10   231.57    -1.79  8500.00     0.00     0.00
 18  9000.00   322.46   241.70     0.25    68.27   310.08   241.81    -2.04  9500.00     0.00     0.00
 19 10000.00   279.41   235.20     0.16    51.28   303.49   252.21    -2.17 10500.00     0.00     0.00
 20 11000.00   241.15   228.80     0.06    36.36   298.38   262.02    -1.45 11500.00     0.00     0.00
 21 12000.00   207.25   222.30     0.02    26.76   294.60   267.85    -0.48 12500.00     0.00     0.00
 22 13000.00   177.38   216.90     0.01    22.38   291.91   269.53    -0.06 13500.00     0.00     0.00
 23 14000.00   151.47   215.80     0.00    20.52   290.23   269.72    -0.16 14500.00     0.00     0.00
 24 15000.00   129.29   215.80     0.00    19.06   289.19   270.13    -0.26 15500.00     0.00     0.00
 25 16000.00   110.36   215.80     0.00    17.72   288.43   270.71    -0.29 16500.00     0.00     0.00
 26 17000.00    94.19   215.80     0.00    16.49   287.76   271.27    -0.29 17500.00     0.00     0.00
 27 18000.00    80.41   216.00     0.00    15.41   287.15   271.74    -0.32 18500.00     0.00     0.00
 28 19000.00    68.67   217.00     0.00    14.44   286.63   272.18    -0.43 19500.00     0.00     0.00
 29 20000.00    58.69   218.20     0.00    13.52   286.22   272.70    -0.57 20500.00     0.00     0.00
 30 21000.00    50.20   219.40     0.00    12.63   285.89   273.27    -0.70 21500.00     0.00     0.00
 31 22000.00    42.98   220.60     0.00    11.77   285.63   273.86    -0.84 22500.00     0.00     0.00
 32 23000.00    36.83   221.80     0.00    10.96   285.44   274.48    -0.97 23500.00     0.00     0.00
 33 24000.00    31.58   223.00     0.00    10.23   285.31   275.08    -0.75 24500.00     0.00     0.00
 34 25000.00    27.11   224.20     0.00     9.75   285.23   275.48    -1.89 27500.00     0.00     0.00
 35 30000.00    12.86   234.20     0.00     6.62   285.28   278.66    -3.82 32500.00     0.00     0.00
 36 35000.00     6.31   245.30     0.00     4.24   285.87   281.63    -5.99 37500.00     0.00     0.00
 37 40000.00     3.20   257.50     0.00     2.61   286.45   283.84    -8.85 42500.00     0.00     0.00
 38 45000.00     1.67   269.70     0.00     1.44   286.88   285.44   -12.25 47500.00     0.00     0.00
 39 50000.00     0.89   276.20     0.00     0.54   287.10   286.57    -3.06 60000.00     0.00     0.00
 40 70000.00     0.06   219.10     0.00     0.02   286.88   286.87    -0.07 87000.00     0.00     0.00
 41104000.00     0.00   209.90     0.00     0.00   286.87   286.87    -1.86152000.00     0.00     0.00
 Note: IEEE floating-point exception flags raised:
    Inexact;  Underflow;
 See the Numerical Computation Guide, ieee_flags(3M)
kruuna.helsinki.fi%
```